Journal of Geodesy (2020) 94:89
https://doi.org/10.1007/s00190-020-01416-1

ORIGINAL ARTICLE

Estimation of frequency and duration of ionospheric disturbances over Turkey with IONOLAB-FFT algorithm

Secil Karatay[1]

Received: 2 September 2019 / Accepted: 6 August 2020 / Published online: 31 August 2020

Abstract
One of the more common methods of observation of variability of the Earth's ionosphere is based on total electron content (TEC) estimated from ground-based dual-frequency Global Positioning System (GPS) receivers. Variations in solar, geomagnetic and seismic activity cause depletions or enhancements in the ionospheric electron concentrations that can be detected as disturbances. Some of these disturbances have wave-like characteristics, where frequency of oscillation can be used to identify and classify the disturbance. In this study, the frequency of such periodic disturbances is estimated using a fast Fourier transform (FFT)-based method, namely IONOLAB-FFT, in the spectral domain. IONOLAB-FFT, which was initially developed to be used on slant TEC (STEC), is modified to be applied to TEC in the local zenith direction of the receiver. The algorithm is tested using literature data on disturbances generated by a geomagnetic activity, a solar flare, a medium-scale traveling ionospheric disturbance (MSTID), a large-scale TID (LSTID) and an earthquake. An accordance with these known disturbances is observed in running IONOLAB-FFT, and the main frequencies and durations of the disturbances are estimated. IONOLAB-FFT method is applied to TEC computed from Turkish Permanent GPS Network (TNPGN-Active) which lies in mid-latitude region to detect the any wave-like oscillations, sudden disturbances and other irregularities during December, March, June and September months for 2010, 2011 and 2012 years. It is observed that a large number of the estimated frequencies are accumulated between 0.08 and 0.14 MHz corresponding to periods of 3.5 h to 2 h. The significant frequencies are grouped less than 0.28 MHz. A large number of the durations of the oscillations are between 425 and 550 min in 2010, 300 and 550 min in 2011 and 350 and 400 min in 2012. The longest duration (around 800 min: 13.33 h) is observed in December months, and the shortest duration (around 2 h) is observed in September months.

Keywords Ionosphere · GPS · Total electron content · Disturbances · FFT

1 Introduction

The ionosphere is defined as the region of Earth's upper atmosphere between 50 and 1000 km. It has electrically charged ions and electrons that affect the propagation of radio waves. The charged particles are produced mainly by solar radiation. Therefore, the properties of the ionosphere depend significantly on the Sun and its activity. The ionization in the ionosphere varies with in space and time. A 11-year solar cycle and seasonal, monthly and diurnal periodicities are the characteristics of the ionosphere. The other mechanism and factors, such as solar, geomagnetic and seismic activities, disturb the ionosphere and affect the level of ionization (Davies and Baker 1965; Rishbeth and Garriott 1969; Banks and Kockarts 1973; Fejer et al. 1979; Pi et al. 2000; Rishbeth and Mendillo 2001; Kil et al. 2003; Lastovicka 2009; Karatay et al. 2010, 2017; Sagir et al. 2015). Temporal and spatial variations of the ionosphere generally depend on the daily and annual rotations of the Earth and the distribution of magnetic field lines. Ionosphere is quiet or disturbed depending on solar and geomagnetic activities. Various geomagnetic and solar indices are utilized to discriminate the deviations from the quiet conditions.

The most important parameter characterizing the ionosphere is the electron density. Total electron content (TEC), which is defined as the line integral of the electron density on ray path, is one of the commonly used observables of ionosphere. The unit of TEC is TECU, where 1 TECU is equal to 10^{16} electrons/m^2 (Arikan et al. 2003, 2007). Global Posi-

✉ Secil Karatay
skaratay@kastamonu.edu.tr

[1] Department of Electrical and Electronics Engineering, Kastamonu University, Kastamonu, Turkey

tioning System (GPS) provides a cost-effective means for the estimation of TEC with worldwide dual-frequency receivers (Nayir et al. 2007; Sezen et al. 2013). The research on ionospheric TEC and its disturbances is also advantageous to further improve and enhance the correction and modeling performance of the ionospheric TEC closely related to precise satellite navigation and positioning (Klobuchar 1987; Prieto-Cerdeira et al. 2014; Roma-Dollase et al. 2018; Yuan et al. 2019).

For a long time, it has been observed that the variations in solar, geomagnetic and seismic activity cause deviations from the quiet conditions of the ionosphere. A large number of studies in the literature suggest that geomagnetic storms, solar activity, higher numbers of sunspot numbers (SSN) and solar flares (SFs) can cause strong disturbances in the electron density distribution and TEC (Rishbeth and Garriott 1969; Biqiang et al. 2007; Vlasov et al. 2003; Zhang and Xiao 2003). During a geomagnetic storm, space weather becomes more vulnerable, and thus, some of the most severe geomagnetic storms such as St Patrick Day storm (March 17–21, 2015), Halloween Storm (October 29–November 3) and 24–26 October 2011 storm were observed. During high SSN years and summer season, the ionization increases, and as a result, the diurnal dynamic range of TEC can reach 40 TECU for mid-latitude regions. Solar flare events are accepted to be one of the most intensive disturbers of the space weather. During SFs, the Sun lets out high-energy protons and electrons and increases the radiation in all wavelengths that affect the propagation of radio waves. A sudden increase in the EUV emission during SFs causes a sudden enhancement of the ionization that can last from minutes to hours (Yasyukevich et al. 2018). Many studies on the ionospheric response have been related to the level of impact of SFs (Afraimovich 2000; Sripathi et al. 2013; Tsurutani et al. 2005; Yasyukevich et al. 2018). In recent years, many studies such as Karatay et al. (2010), Pulinets et al. (2005, 2007) and Liu et al. (2004) suggest that pre-, co- and post-seismic activity may affect the ionospheric structure, such as electron density, ion density, critical frequencies of the ionospheric layers, ion temperatures and TEC.

Some of the ionospheric irregularities occur as wave-like oscillations. In the literature, traveling ionospheric disturbances (TIDs) make up of a large group of such oscillatory, propagating plasma irregularities (Hocke and Schlegel 1996; Shiokawa et al. 2003; Katamzi et al. 2012). These disturbances can travel several thousand kilometers, and their speeds can reach to some hundreds of kilometers per hour (Rishbeth and Garriott 1969). TIDs are further grouped into medium-scale TID (MSTID) (Fedorenko et al. 2011; Husin et al. 2011; Hernandez-Pajares et al. 2006; Hocke and Schlegel 1996) and large-scale TID (LSTID) (Francis 1973; Nicolls et al. 2004; Ding et al. 2007). MSTIDs have horizontal wavelengths of several hundred kilometers, horizontal velocities of 100 to 250 m/s and periods of 15 to 60 min (Hocke and Schlegel 1996; Tsugawa et al. 2007; Hernandez-Pajares et al. 2006). LSTIDs have periods of 1 to 3 h and horizontal wavelengths of 1,000 to 4000 km, with velocities above 300 m/s. They are considered to be a manifestation of atmospheric gravity waves excited by sources in polar regions of the northern and southern hemispheres (Tsugawa et al. 2007; Ding et al. 2007). These kinds of disturbances are among the major causes of positioning and navigational errors in GPS-based autonomous systems (Krankowski et al. 2005; Stankov et al. 2009; Jakowski et al. 2012; Bergeot et al. 2014; Efendi and Arikan 2017; Arikan and Yarici 2017). Except some limited number studies such as IONOLAB-FFT (Arikan and Yarici 2017), there is no systematic method that can detect and classify the frequency and duration of wave-like disturbances over TEC in the literature.

In the literature, ionospheric disturbances are typically investigated with temporal derivative-based methods on total electron content data estimated from Global Positioning System receivers (GPS-TEC) (Ho et al. 1998; Yuan and Ou 2001a, b; Zhang and Xiao 2003; Krankowski et al. 2006; Cherniak et al. 2014; Efendi and Arikan 2017). In Hargreaves (1992), the effects of TIDs are observed from electron content measurements from two geostationary satellites received at a single ground station. A downward movement of gravity waves and an average TID producing 1% variation in TEC have been observed in this study. The magnetospheric electric fields accompanied by TEC fluctuations can be as large as ± 5 TECU and saturated 250 MHz scintillations in near-solar maximum condition that may affect the GPS systems in the mid-latitude region (Basu et al. 2001). The combination of the equatorward movement of the ionospheric trough, along with a storm time-enhanced density disturbance, can degrade or even distort the navigation systems and ionospheric radio wave propagation (Ledvina et al. 2002). The geomagnetic storms are also a driver of TIDs as given in various studies in the literature such as Davis (1971), Basu et al. (2001), Zhang and Xiao (2003), Krankowski et al. (2005), Tsugawa et al. (2007) and Ding et al. (2007, 2008).

The Fourier transform is a frequency domain representation of any periodic function defined in the time domain. The discrete Fourier transform (DFT) is applied to divide a signal into its frequency components over a period of time or space. The fast Fourier transform (FFT) is an algorithm that is widely used for calculating DFT.

In this study, an FFT algorithm, namely IONOLAB-FFT, is used to estimate possible frequency components on TEC and identify major components that consists of a significant portion of the spectrum. IONOLAB-FFT is developed in Arikan and Yarici (2017) for the first time, and it is applied to slant TEC (STEC) values. STEC corresponds to the total number of electrons on the ray path between a GPS satellite and a ground-based receiver. The accuracy and reliability

of IONOLAB-FFT are tested over a set of simulations that model possible TID wave-like oscillations, characterized by their amplitude, duration and frequency. In Arikan and Yarici (2017), it is concluded that the frequency estimates of the algorithm can be determined with an accuracy better than 80% for frequencies from 0.6 to 2.4 MHz and durations longer than 10 min; for frequencies from 0.15 to 0.6 MHz and durations longer than 50 min; and for frequencies higher than 0.29 MHz and durations longer than 50 min.

In this study, IONOLAB-FFT is applied to GPS-TEC instead of STEC for the first time in the literature. In the first step, the data are smoothed and its trend is estimated using a set of moving median filters. Then, the algorithm of IONOLAB-FFT is applied similar to that in Arikan and Yarici (2017). The application of the algorithm on GPS-TEC is demonstrated on a quiet day as well as for disturbances that result from an SF, a geomagnetic storm and an earthquake, which are well documented in the literature. Finally, IONOLAB-FFT is applied to selected stations from a mid-latitude GPS network and most common frequency components are tabulated. This study is one of the first applications of a systematic study in analysis of wave-like plasma irregularities using spectral methods.

The modified IONOLAB-FFT algorithm and the data used in the study are presented in Sects. 2 and 3. The results are given in Sect. 4.

2 IONOLAB-FFT algorithm for IONOLAB-TEC

In this study, IONOLAB-FFT algorithm, which is developed for the wave-like disturbances on STEC in Arikan and Yarici (2017), is modified to be applied to GPS-TEC data. In Arikan and Yarici (2017), the trend structure was removed using a least-squares fit to a linear function due to the fact that STEC values are increasing and/or decreasing as the GPS satellites move in orbit. The expected structural trend of TEC in local time is very different from that of STEC values. Therefore, the removal of trend structure for TEC is modified in this study using two sliding window median filters.

The TEC data estimated for the day d can be expressed as in Eq. 1 with receiver number u, total number of measurements N and sample number n as:

$$\boldsymbol{x}_{u;d} = \left[x_{u;d}(1) \ldots\ldots\ldots x_{u;d}(n) \ldots\ldots\ldots x_{u;d}(N)\right]^T \quad (1)$$

where $1 \leq n \leq N$ and T denote the transpose operator. Example of IONOLAB-TEC for anrk station located in Ankara, Turkey, at 39.86 N and 32.85° E is given in Fig. 1a as a solid black line for the geomagnetically quiet day on March 09, 2010.

In the digital signal/image processing, a median filter defined as a nonlinear digital filtering technique is often used to remove or smooth the noise from an image or a signal. A median filter is used to reduce the random noise when the noise amplitude probability has large tails and periodic patterns. The median filtering process is performed by a sliding window over the signal or image (Ohki et al. 1995). TEC may have irregularities or sudden data disruptions that may not be directly related to disturbances in the ionosphere. Therefore, the TEC data are filtered with a moving median filter of length T_{f1} as:

$$\boldsymbol{a}_{u;d} = \text{medfilt}\left(\boldsymbol{x}_{u;d}, T_{f1}\right) \quad (2)$$

In this study, T_{f1} is chosen to be 12.5 min. This time duration is slightly smaller than the period of a MSTID (which is reported to be 15 min to 1 h in the literature as given in the previous section). At the same time, this value of T_{f1} corresponds to the wide-sense stationarity period of mid-latitude ionosphere as discussed in Sayin et al. (2010) and Erol and Arikan (2005). After 10 min, the ionosphere over mid-latitudes starts to be de-correlated temporally depending on the local zenith. Example of de-noised IONOLAB-TEC, $\boldsymbol{a}_{u;d}$, for anrk station is given in Fig. 1a as a dashed red line. For a quiet day, $\boldsymbol{a}_{u;d}$ is very similar to $\boldsymbol{x}_{u;d}$ as given in Fig. 1a.

In order to estimate the trend of structure of de-noised TEC, a second sliding window median filter of length T_{f2} is applied as follows:

$$\boldsymbol{Y}_{u;d} = \text{medfilt}\left(\boldsymbol{a}_{u;d}, T_{f2}\right) \quad (3)$$

In this study, T_{f2} is chosen to be 4.2 h (or 252 min) since it is observed that this duration is appropriate in representation of TEC trend for mid-latitude ionosphere. Also, as summarized in the previous section, the period of LSTIDs is usually less than 4 h. The estimated de-noised TEC trend, $\boldsymbol{Y}_{u;d}$, is given in dotted green line in Fig. 1a. As shown in Fig. 1a, $\boldsymbol{Y}_{u;d}$ and $\boldsymbol{x}_{u;d}$ differ from each other only for the periods where TEC deviates from expected diurnal trend. These sections are indicated between blued dashed vertical lines in Fig. 1a in roman numerals of I (02.00–04.00 UT), II (10.00–15.00 UT) and III (16.00–22.00 UT). The structure of GPS-TEC and the method of trend estimation using a moving median filter in this study are different from those in Arikan and Yarici (2017) for application of IONOLAB-FFT on STEC data.

Using Eqs. (2) and (3), the difference, $\boldsymbol{D}_{f_{u;d}}$, is obtained as:

$$\boldsymbol{D}_{f_{u;d}} = \boldsymbol{a}_{u;d} - \boldsymbol{Y}_{u;d} \quad (4)$$

Example of the difference, $\boldsymbol{D}_{f_{u;d}}$, is given in Fig. 1b. Possible disturbance periods are indicated with vertical dashed blue lines in Fig. 1b.

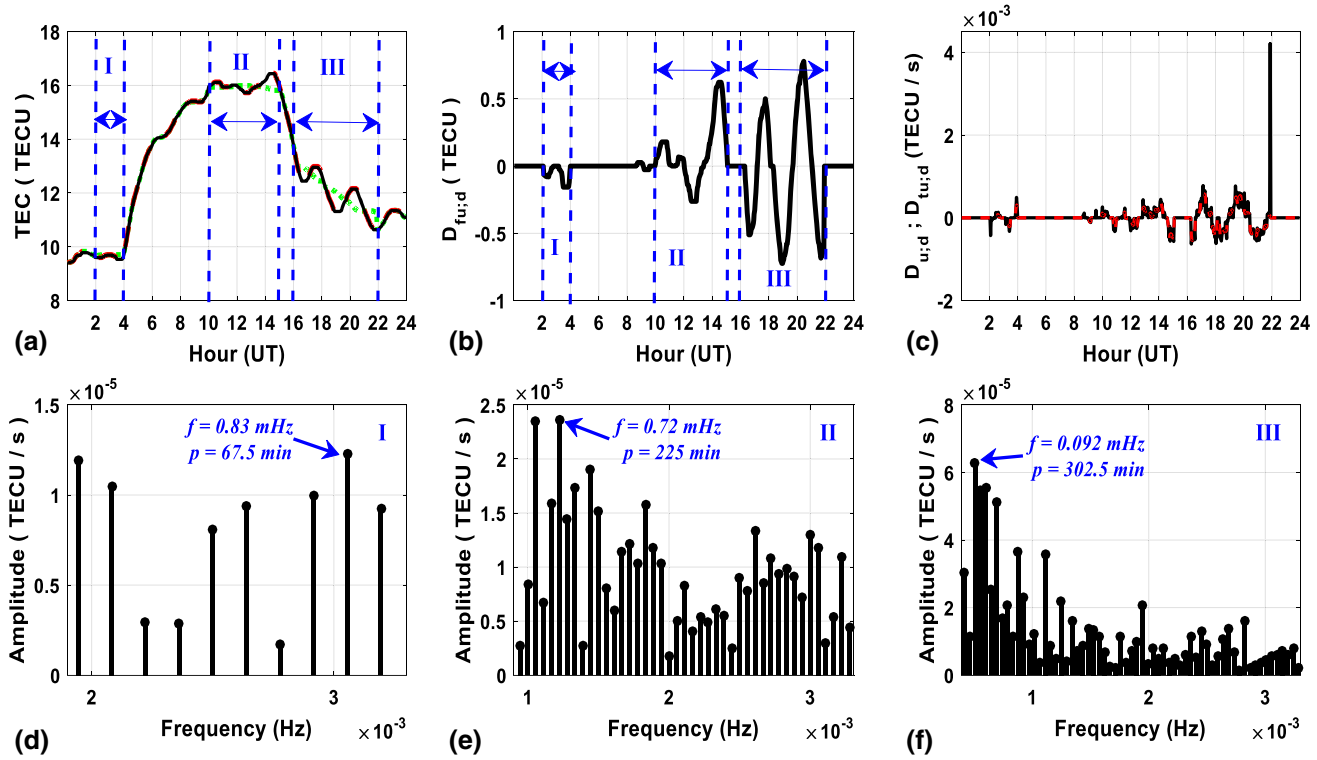

Fig. 1 For the geomagnetically quiet day on March 09, 2010, for GPS station anrk: **a** IONOLAB-TEC (solid black line), denoised IONOLAB-TEC, $\boldsymbol{a}_{u;d}$ (dashed red line) and estimated denoised TEC trend, $\boldsymbol{Y}_{u;d}$ (dotted green line); **b** the difference $\boldsymbol{D}_{f_{u;d}}$; **c** the temporal derivative, $D_{u;d}$, (solid black line) and the smoothed derivative of the difference, $\boldsymbol{D}_{t_{u;d}}$ (dashed red line). The spectrum, $\boldsymbol{F}_{u;d}$, for the most dominant frequency components for: **d** Section I; **e** Section II and **f** Section III, all denoted in part **a**

The temporal derivative of the difference in Eq. 4 is computed as:

$$D_{u;d}(n) = \frac{\left(D_{f_{u;d}}(n+1) - D_{f_{u;d}}(n)\right)}{\Delta t} \tag{5}$$

where Δt is $2.5 \times 60 = 150$ s in this study. Example of the temporal derivative of the difference, $\boldsymbol{D}_{\boldsymbol{u;d}}$, is given with black solid line in Fig. 1c.

In order to reduce the seemingly insignificant variability, the smoothed derivative of the difference, $\boldsymbol{D}_{t_{u;d}}$, is computed in Eq. 6 as given with dashed red line in Fig. 1c. The smoothing is achieved by a third moving median filter with filter length, T_{f3}, as follows

$$\boldsymbol{D}_{t_{u;d}} = \text{medfilt}\left(\boldsymbol{D}_{u;d}, T_{f3}\right) \tag{6}$$

T_{f3} is chosen to be 7.5 min.

In this study, in order to determine the durations of the disturbances, the maximum value of the absolute value, $\left|D_{u;d}(n)\right|$, is computed over all data in a day. Then, 1% of the maximum value is accepted as the threshold. The index of the first value over the threshold is used as the starting point of the threshold. The value $p_{u;d}(1)$ is taken as the first value of the new difference derivative, $\boldsymbol{D}_{p_{u;d}}$ as given in Eq. (7). The final value $p_{u;d}\left(N_p\right)$ of $\boldsymbol{D}_{p_{u;d}}$ is obtained for those components where all absolute values are under the threshold, where $1 \le n_p \le N_p$. At this step, N_p is the duration that has $\boldsymbol{D}_{u;d}$ values whose magnitude is within 1% of the maximum absolute amplitude as follows:

$$\boldsymbol{D}_{p_{u;d}} = \left[p_{u;d}(1) \ldots p_{u;d}\left(n_p\right) \ldots p_{u;d}\left(N_p\right)\right]^T \tag{7}$$

where $p_{u;d}$ denotes the durations for station u and day d. The DFT algorithm is applied to $\boldsymbol{D}_{t_{u;d}}$ as explained in the next subsection.

2.1 Extraction of frequency components using IONOLAB-FFT

The discrete Fourier transform of $\boldsymbol{D}_{t_{u;d}}$ is numerically computed using the fast Fourier transform algorithm as:

$$\boldsymbol{F}_{u;d} = \text{FFT}\left(\boldsymbol{D}_{t_{u;d}}\right) \tag{8}$$

and $\boldsymbol{F}_{u;d}$ is represented as:

$$\boldsymbol{F}_{u;d} = \left[F_{u;d}\left(\frac{1}{N_{u;d}}\right) \dots F_{u;d}\left(\frac{n_\mathrm{f}}{N_{u;d}}\right) \dots F_{u;d}\left(\frac{N_\mathrm{f}}{N_{u;d}}\right) \right]^T \tag{9}$$

where N_f and n_f denote the data length and sample number in frequency domain ($1 \leq n_\mathrm{f} \leq N_\mathrm{f}$), respectively. An example of FFT of $\boldsymbol{D}_{t_{u;d}}$, $\boldsymbol{F}_{u;d}$, is provided in Fig. 1d corresponding to the FFT of Section I in Fig. 1a.

The steps of the algorithm to extract significant frequency components of the possible disturbances are the same as those of IONOLAB-FFT as detailed in Arikan and Yarici (2017). In order to determine the most significant frequency components of the smoothed derivative spectrum, IONOLAB-FFT algorithm in Arikan and Yarici (2017) introduces a loop to the n_L loop counter in order to obtain the frequency components that correspond to highest power. First, the largest magnitude component of the data in frequency domain is obtained for $n_\mathrm{L} = 1$ as follows:

$$a_{u;d}(1) = \max\left(\left|\boldsymbol{F}_{u;d}\right|\right) \tag{10}$$

Finding the inflection point associated with the largest magnitude, the main lobe is estimated. The estimated main lobe can be defined as:

$$\boldsymbol{S}_{u;d}(1) = \left[|S_{u;d}(1)|e^{-j\Phi_1} \dots |S_{u;d}(n_\mathrm{s})|e^{-j\Phi_{n_\mathrm{s}}} \dots |S_{u;d}(N_\mathrm{s})|e^{-j\Phi_{N_\mathrm{s}}} \right]^T \tag{11}$$

where Φ denotes the phase in the main lobe, $\left|S_{u;d}(1)\right|$ denotes the magnitude of the components in the main lobe and N_s denotes the total sample size in the main lobe ($1 \leq n_\mathrm{f} \leq N_\mathrm{f}$). The components in the estimated main lobe can be defined as sinusoidal functions as:

$$S_{u;d}(n;1) = \sum_{n_\mathrm{s}=1}^{N_\mathrm{s}} \left(\left|S_{u;d}(n_\mathrm{s})\right| \frac{\mathrm{Cos}\, f(n_\mathrm{s})n}{N} + \Phi(n_\mathrm{s}) \right) \tag{12}$$

Here, f denotes the main frequency in the main lobe. By the sum of these sine functions, the percentage of the normalized total difference is obtained with derivative data in Eq. 5 as follows:

$$e_{u;d}(1) = \frac{\left|\boldsymbol{D}_{u;d} - \boldsymbol{S}_{u;d}(1)\right|_2}{\left|\boldsymbol{D}_{u;d}\right|_2} \times 100 \tag{13}$$

Here, $|.|_2$ denotes L_2 norm or metric norm. At this step, if $e_{u;d}(1) \geq 40\%$, the estimated main lobe is extracted from spectrum in the frequency domain given in:

$$\boldsymbol{G}_{u;d}(1) = \left|\boldsymbol{F}_{u;d}\right| - \boldsymbol{S}_{u;d}(1) \tag{14}$$

Then, the algorithm returns to Eq. 10 using $\boldsymbol{G}_{u;d}$ and the loop continues until $e_{u;d} < 40\%$. The most significant frequencies are organized as:

$$\boldsymbol{f}_{\boldsymbol{u;d}} = \left[f_{u;d}(1) \dots f_{u;d}(n_L) \dots f_{u;d}(N_L) \right]^T \tag{15}$$

As given in Fig. 1d, the most significant frequency in Section I of Fig. 1a is 0.83 MHz and the duration, p, is 67.5 min. In Fig. 1e, the frequency spectrum for Section II in Fig. 1a is shown and the most significant frequency is 0.72 MHz, and the duration is 225 min (3.75 h). In Fig. 1f, the frequency spectrum for Section III in Fig. 1a is given with the most significant frequency components of 0.092 MHz and duration 302.5 min (5.04 h). On a quiet day, some disturbances or irregularities on TEC can be observed with lower frequencies and periods longer than 1 h as shown in Fig. 1f.

The IONOLAB-FFT algorithm can be applied to full day (24 h) TEC data or a section of TEC data where possible disturbances are observed. When IONOLAB-FFT is applied to the whole day TEC in Fig. 1a, the dominant frequency and the duration are 0.54 MHz and 530 min (8.83 h), respectively.

As a summary, the general flow of the IONOLAB-FFT algorithm can be summarized as follows:

1. De-noising and smoothing TEC and estimation of its trend using moving median filters (Eqs. 2 and 3);
2. Calculation of difference of TEC between its de-noised and smoothed trend (Eq. 4);
3. Computation of the derivative of difference (Eq. 5);
4. Reducing the noise-like components with a third sliding window median filter and computation of $\boldsymbol{D}_{t_{u;d}}$ (Eq. 6);
5. Collection of the most significant variabilities on the derivative of the difference in $\boldsymbol{D}_{p_{u;d}}$ and estimation of the duration (p) of the disturbance (Eq. 7);
6. Computation of FFT of $\boldsymbol{D}_{t_{u;d}}$ (Eq. 8);
7. Extraction of the largest amplitude components of the spectrum and the main lobes associated with these largest amplitudes one by one;
8. Summation of the sine functions that correspond to the largest amplitude frequency components;
9. Termination of the loop when the difference between the sum of sine functions and the original spectrum is within a predetermined power limit.

In the next section, the data used in the study are given. In Sect. 4, IONOLAB-FFT is first applied to the five special ionospheric events and then it is applied to TEC data obtained from stations located in Turkey for equinox and solstice months of 2010–2012.

Table 1 Dates of events, state of the ionosphere and GPS stations that are used in application of IONOLAB-FFT

Event	Date	Ionospheric state	GPS stations
1	September 08, 2017	Geomagnetically disturbed	anrk (39.86 N, 32.85 E)
2	September 06, 2017	Sudden ionospheric disturbance due to SF (Yasyukevich et al. 2018)	djig (11.45 N, 42.84 E)
3	October 29, 2003	Large-scale traveling ionospheric disturbance (Ding et al. 2007, 2008; Wang et al. 2007; Efendi and Arikan 2017)	colb (39.77 N, 83.04 W) pktn (38.85 N, 83.02 W) coso (35.98 N, 117.81 W)
4	July 20, 2006	Medium-scale traveling ionospheric disturbance (Tsugawa et al. 2007; Efendi and Arikan 2017)	ccv3 (28.29 N, 80.54 W) pit1 (40.36 N, 79.69 W) kyw1 (24.43 N, 81.65 W)
5	May 12, 2008	Seismic activity (Wenchuan earthquake) (Jin et al. 2010; Hsiao et al. 2010; Karatay et al. 2010; Lin 2014; Jianyong et al. 2015; Song et al. 2015)	kunm (24.88 N, 102.79 E) lhaz (29.49 N, 91.104 E) xian (34.88 N, 109.22 E)

3 Data

In this study, TEC estimated from dual-frequency GPS receivers is used as the data source. TEC values are obtained as IONOLAB-TEC. IONOLAB-TEC that is based on regularized estimation (Reg-Est) algorithm is one of the most robust, reliable and accurate algorithms in the literature for estimation of GPS-TEC over a single station in the local zenith direction from dual-frequency GPS receivers as detailed in Arikan et al. (2003,2004). The state-of-the-art Reg-Est algorithm fuses the vertical TEC values at the same epoch but at different ionospheric pierce points (IPPs) and estimates TEC at the local zenith direction of the GPS receiver. The algorithm makes use of the satellite ephemeris data obtained from ftp://cddis.gsfc.nasa.gov/gps/products/ionex/. The necessary satellite differential code biases (DCBs) are downloaded from the same site listed in IONospheric EXchange (IONEX) files. The receiver DCBs are calculated using IONOLAB-BIAS algorithm as given in Arikan et al. (2008). As detailed in Arikan et al. (2008), the ground truth in bias computation is obtained from International GNSS Service (IGS) products, namely Center for Orbit Determination (CODE) Global Ionospheric Map (GIM) TEC (for Europe) or Jet Propulsion Laboratory (JPL) GIM-TEC (for the rest of the world). Although we realize there are recent papers that investigate the intraday variability of ionosphere reflected into receiver DCB (including but not limited to Sardon et al. 1994; Brunini et al. 2011; Coster et al. 2013; Zhang et al. 2017; Zhang et al. 2018), our algorithm still keeps the receiver DCB constant during a day similar to the assumptions of IGS Ionospheric Analysis Centers. In Nayir et al. (2007), it has been shown that IONOLAB-TEC estimates using Reg-Est algorithm are robust to the choice of IPP heights and the methods for ambiguity resolution in leveled phase-delay computation.

IONOLAB-TEC is also available as an online space weather service at www.ionolab.org (Sezen et al. 2013). The current version of IONOLAB-TEC can be used online or can be downloaded from www.ionolab.org site as *.exe format (Arikan et al. 2016). In this study, IONOLAB-STEC values are estimated with 30-s time resolution and IONOLAB-TEC values are obtained with 2.5-min time resolution (Arikan et al. 2016).

In this study, initially, IONOLAB-FFT method is applied to IONOLAB-STEC and IONOLAB-TEC data from chosen GPS stations given in Table 1 on known days of disturbance. The events represent various days of solar, geomagnetic and seismic activity. Geomagnetic storm days are obtained from Pushkov Institute of Terrestrial Magnetism, Ionosphere and Radio Wave Propagation Russian Academy Sciences at https://www.izmiran.ru/ionosphere/weather/storm/. The disturbed and quiet day lists are obtained from Regional Warning Center Warsaw (RWC). The Ionospheric Dispatch Center in Europe (IDCE) disturbance lists are obtained from Space Research Center of Poland (PAS) at ftp://ftp.cbk.waw.pl/idce/quiet_days/q_d_days.ctl. Earthquake days are obtained from https://earthquake.usgs.gov/earthquakes. The geomagnetic indices Kp and Ap and sunspot number (SSN) are obtained from Space Weather Prediction Center (ftp://ftp.swpc.noaa.gov/pub/indices/old_indices/). Hourly values of Dst and AE indices are obtained from World Data Center for Geomagnetism (https://wdc.kugi.kyoto-u.ac.jp/dstdir/).

September 08, 2017, indicated as Event 1 in Table 1, is a geomagnetic storm day. On this disturbed day, Kp increased to 8 and this state lasted for 3 h. Dst index had a minimum value of − 124 nT. The maximum value of AE and Ap indices was 1442 nT and 96, respectively. The quarterly daily values of SSN on March 09, 2010, and September 09, 2017, are 0 and 89, respectively. Event 1 is also investigated over anrk station.

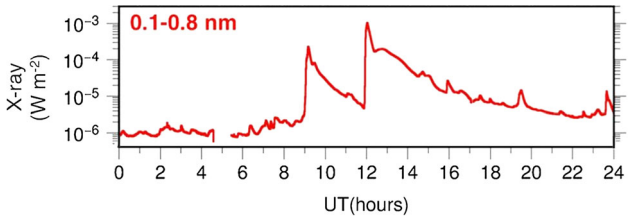

Fig. 2 X-ray irradiance in the range 0.1–0.8 nm as measured by GOES-13 satellite at 1 AU on September 06, 2017 (https://satdat.ngdc.noaa.gov/; Yasyukevich et al. 2018)

For the Event 2 in Table 1, a reported sudden ionospheric disturbance (SID), which was observed as a result of significant SFs on September 06, 2017 (Yasyukevich et al. 2018), is investigated to determine the frequency and the duration of the disturbance. On September 06, 2017, the Sun emitted two significant SFs. The first SF, classified X2.2, peaked at 09.10 UT. The second one, X9.3, which is the most intensive SF in the current solar cycle, peaked at 12.02 UT (https://www.spaceweatherlive.com/en/archive/2017/09/06/xray; Yasyukevich et al. 2018). X-ray irradiance as measured by GOES-13 satellite on September 06, 2017, is given in Fig. 2 Event 2 is investigated over djig GPS station located at (11.45° N, 42.84° E), Djibouti, Somalia.

The IONOLAB-FFT method is also applied to two types of TID events, which are specifically mentioned in Ding et al. (2007, 2008), Tsugawa et al. (2007), Wang et al. (2007) and Efendi and Arikan (2017). Event 3 in Table 1 occurred during the period of October 29 to November 01, 2003, Halloween Storm. The geomagnetic storms were accompanied by LSTIDs observed in North America on October 29, 2003, between 06.20 and 08.00 UT (Ding et al. 2007, 2008; Wang et al. 2007; Efendi and Arikan 2017). Maximum value of Kp index was 9, and this value lasted for 3 h. During this period, the Dst index had a minimum value of − 350 nT. The maximum value of the AE index was 2241 nT and Ap index was 189. This event was investigated over colb (39.77° N, 83.04° W), Columbus, USA; pktn (38.85° N, 83.02° W), Piketon, USA; and coso at (35.98° N, 117.81° W), Coso Junction, USA. These stations are chosen since they are also used in a network, especially in Ding et al. (2007, 2008), Wang et al. (2007) for the observation of LSTID.

Event 4 in Table 1 corresponds to an MSTID that was observed on July 20, 2006, between 03.30 UT and 06.10 UT over North America (Tsugawa et al. 2007; Efendi and Arikan 2017). On this day, Kp index was less than 1 for the whole day. The lowest value of Dst index was about 1 nT. The maximum value of AE index was 134 nT and Ap index was 3. The GPS stations that are used in investigation of Event 5 are ccv3 (28.29° N, 80.54° W), Cape Caneveral, USA; pit1 (40.36° N, 79.69° W), New Kensington, USA; and kyw1 (24.43 N, 81.65 W), Key West, USA. These stations are also mentioned in Tsugawa et al. (2007) for the observation of reported MSTID.

For Event 5, Wenchuan (Sichuan) earthquake is chosen to detect the frequency and the duration of the ionospheric disturbance during a severe seismic activity. The Sichuan earthquake occurred in China at 06.28 UT on May 12, 2008. The magnitude of the earthquake on Richter scale is recorded as 7.9 Mw. The epicenter of earthquake is located at geographical coordinates 31.02° N and 103.37° E. The available GPS stations surrounding the earthquake epicenter are kunm (24.88 N, 102.79 E), Kunming, China, lhaz (29.49° N, 91.104° E), Lhasa, China, and xian (34.88° N, 109.22° E), Lintong, China, as given in Table 1. On this day, the ionosphere can be considered as quiet. Maximum value of Kp index is 2. The value of Ap index is 4. The effect of co- and post-seismic activity of this earthquake is reported in Jin et al. (2010), Jianyong et al. (2015), Song et al. (2015). The effects of pre-, co- and post-seismic activity of Wenchuan earthquake are presented in Karatay et al. (2010), Hsiao et al. (2010) and Lin (2014).

Secondly, IONOLAB-FFT is applied to five selected stations of Turkish National Permanent GPS Network (TNPGN-Active) (as given in Fig. 3) for December, March, June and September months in low solar active year 2010 and moderate solar active years 2011 and 2012 in order to observe the variability of fundamental frequencies of GPS-TEC.

The position of anrk station located in Ankara, Turkey, is given in Table 1 and Fig. 3. antl GPS station is located in Antalya, Turkey, at (36.89° N, 30.67° E). ardh is Ardahan, Turkey, at (41.11° N, 42.70° E). The GPS station band is at Bandirma, Turkey (40.33° N, 28.00° E). The btmn station, whose coordinates are (37.86° N, 41.15° E), is Batman, Turkey. These stations are chosen as representatives to investigate the anisotropicity of ionosphere in terms of frequencies and durations of wave-like disturbances. In the next section, the IONOLAB-FFT is first applied to the events given in Table 1 and then it is applied to TEC data obtained from stations in Fig. 3 for equinox and solstice months of 2010–2012.

4 Results and discussion

In the first part of this section, the IONOLAB-FFT algorithm is applied to five ionospheric states given in Table 1. September 08, 2017, chosen for Event 1 is a geomagnetic storm day. Three significant irregularities as oscillations are observed between 01.00 UT and 06.00 UT; 07.00 UT and 18.00 UT; and 19.00 UT and 23.00 UT over anrk on this day as given in Fig. 4a, d, g, respectively, indicated by vertical blue dashed lines, and the designated durations are depicted by blue horizontal arrows. The smoothed derivatives of the difference, $\boldsymbol{D}_{t_{u;d}}$ (solid black line), and summed sine functions, $\boldsymbol{S}_{u;d}$ (red solid line), are given in Fig. 4b, e, h for the related dis-

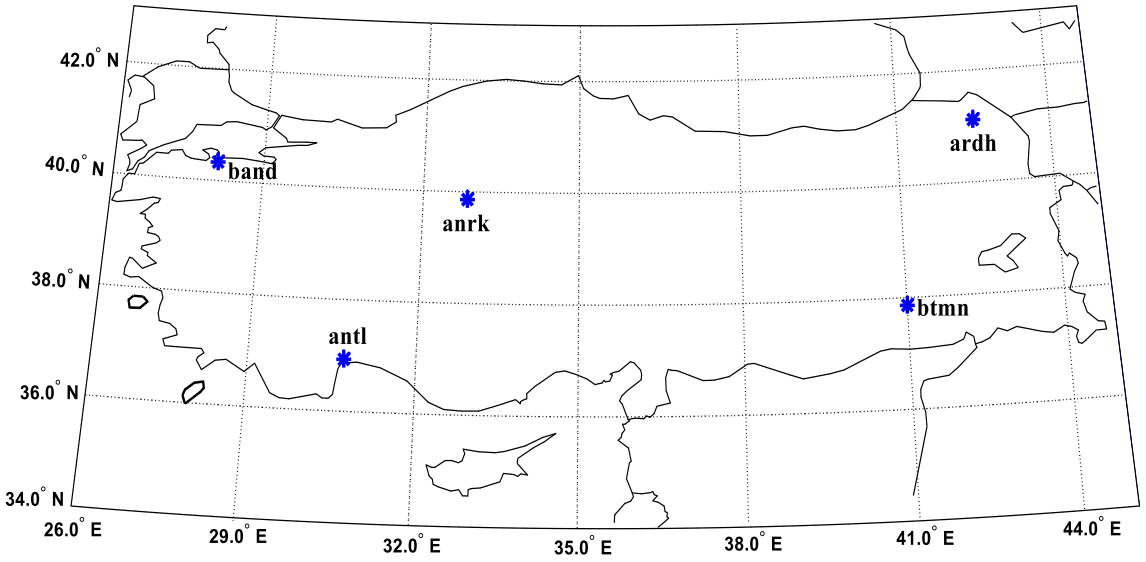

Fig. 3 Chosen TNPGN-Active stations are marked with blue dot

turbance intervals, respectively. The respective spectrums, $\boldsymbol{F}_{u;d}$, are provided in Fig. 4c, f, i. As can be observed from Fig. 4c, f, i, the maximum value of the spectrum is estimated as 0.11 MHz (period is 2.52 h), 0.075 MHz (period is 3.42 h) and 0.48 MHz (period is 34.72 min or 0.578 h) between 01.00 and 06.00 UT, 07.00 and 18.00 UT and 19.00 and 23.00 UT, respectively. The estimated durations of the irregularities are 185.5 min (or 3.09 h), 510 min (or 8.5 h) and 22.5 min, respectively.

The frequency and the duration over 24 h for Event 2 are 0.081 MHz and 665 min (11.08 h), respectively. The scale of the irregularities is significantly larger, and the durations are longer as compared with those given for the geomagnetically quiet day given in Fig. 1.

For Event 2, IONOLAB-FFT is applied to IONOLAB-STEC during SFs. The variability on September 06, 2017, is also investigated on IONOLAB-TEC. The station djig, which is significantly affected by the SFs (Yasyukevich et al. 2018), is used to compute the frequency and the duration of the disturbances. It is observed on the IONOLAB-STEC that the frequency has the lower values when the most intensive SF, peaked at 09.00 UT and 12.00 UT, occurred (Fig. 2). The higher frequencies are observed in the less intensive SF peaked at 16.00 UT. The durations of the disturbances are longer than those of the less intensive SFs. In Fig. 5, IONOLAB-STEC values are provided for all GPS satellites (PRN) that were in view of djig during three SFs time intervals. In Fig. 6a, IONOLAB-TEC is given for all day. The time intervals between 09.00 UT and 12.00 UT, 12.00 UT and 16.00 UT, and 16.00 UT and 20.00 UT are indicated with vertical dashed blue lines. In Fig. 6b, the smoothed derivatives of the difference, $\boldsymbol{D}_{t_{u;d}}$, and summed sine functions, $\boldsymbol{S}_{u;d}$, are given between 09.00 UT and 20.00 UT. In Fig. 6c, the spectrums, $\boldsymbol{F}_{u;d}$, are given for the same time intervals as in Fig. 6b. The significant frequencies and the durations are estimated as:

- Between 09.00 and 12.00 UT; $f = 0.092$ mHz, $p = 117.5$ min (1.95 h)
- Between 12.00 and 16.00 UT; $f = 0.069$ mHz, $p = 167.5$ min (2.79 h)
- Between 16.00 and 20.00 UT; $f = 0.48$ mHz, $p = 22.5$ min (0.37 h)
- Between 09.00 and 20.00 UT; $f = 0.15$ mHz, $p = 302.5$ min (5.03 h)

It is observed that the frequencies computed over IONOLAB-STEC vary between 0.1 and 0.5 MHz while the frequencies computed over IONOLAB-TEC mostly have values smaller than 0.15 MHz. The durations computed over IONOLAB-STEC are longer than those computed for IONOLAB-TEC.

For Event 3, the IONOLAB-FFT method is applied to a well-recognized traveling ionospheric disturbance reported in the literature. October 29, 2003, was the start day of a major geomagnetic disturbance, namely the Halloween Storm. The disturbance was observed as large-scale traveling ionospheric disturbance over North America (Ding et al. 2007, 2008; Wang et al. 2007; Efendi and Arikan 2017). Three GPS stations located in North America are used to estimate the frequency and the duration during LSTID as given in Table 1. The LSTID was observed at GPS stations colb, pktn and coso between 06:20 and 08:00 UT in Ding et al. (2007, 2008), Wang et al. (2007). The IONOLAB-TEC values and the disturbance times for reported LSTIDs are provided in Fig. 7a–c for colb, pktn and coso, respectively.

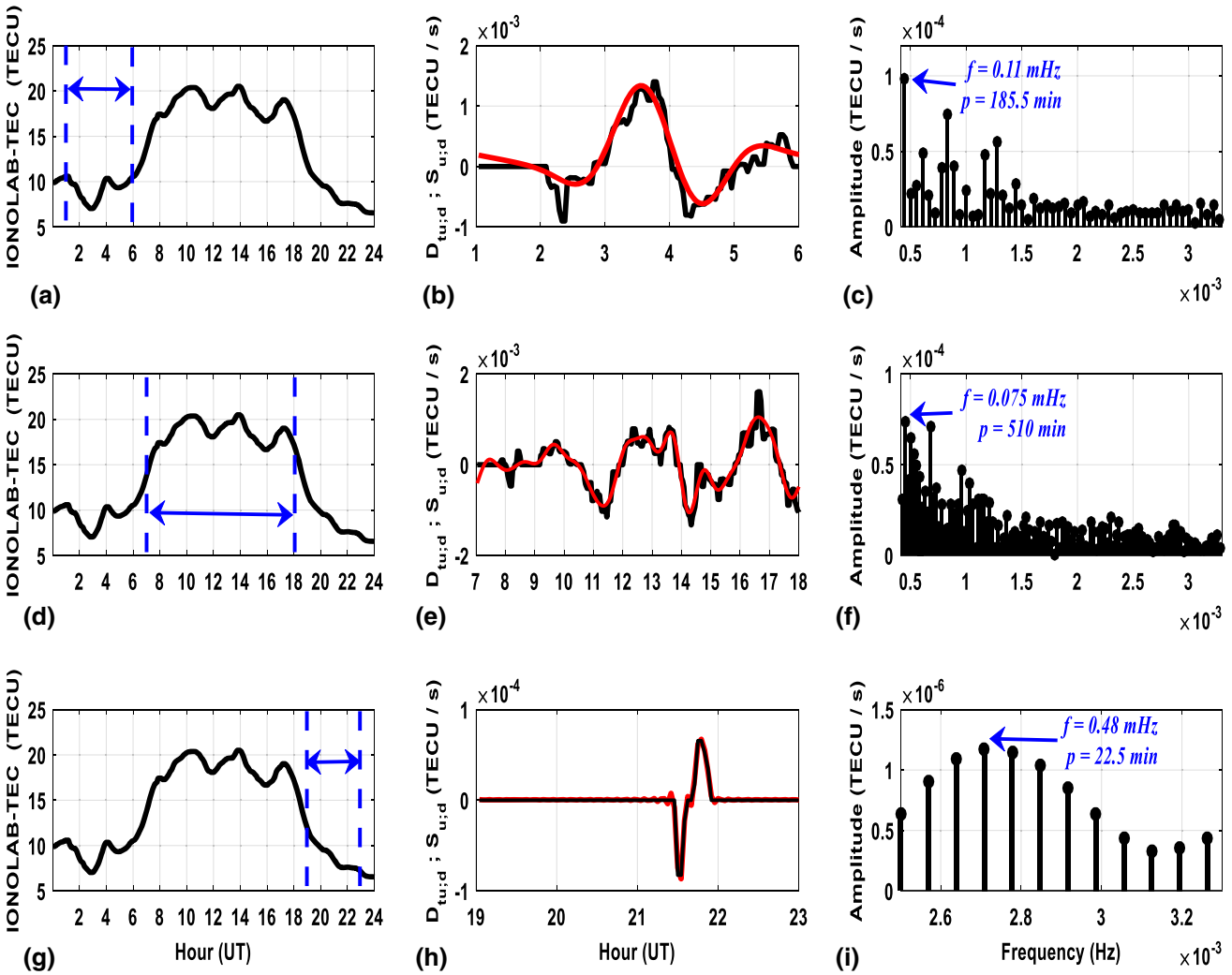

Fig. 4 Event 1, disturbed day, September 08, 2017, for station anrk: **a**, **d** and **g** IONOLAB-TEC, the approximate disturbances are indicated by vertical dashed blue lines and the horizontal blue arrow is the approximate duration of irregularities; the smoothed derivatives of the difference, $\boldsymbol{D}_{tu;d}$, (black) and summed sine functions, $\boldsymbol{S}_{u;d}$, (red) between **b** 01.00 UT and 06.00 UT, **e** 07.00 UT and 18.00 UT, and **h** 19.00 UT and 23.00 UT; the spectrums, $\boldsymbol{F}_{u;d}$, between **c** 01.00 UT and 06.00 UT, **f** 07.00 UT and 18.00 UT, and **i** 19.00 UT and 23.00 UT

For Event 4, an MSTID is detected over North America on July 20, 2006, between 03.30 UT and 06.10 UT as reported in Tsugawa et al. 2007, Efendi and Arikan 2017). There is no existing disturbance due to geomagnetic storm at this day. The MSTID was observed at GPS stations ccv3, pit1 and kyw1 in Tsugawa et al. (2007). IONOLAB-TEC values are provided for ccv3, pit1 and kyw1 in Fig. 7d–f, respectively. Besides the time intervals of the observed LSTID and MSTID, the frequencies and durations are estimated for some other time intervals when some irregularities are observed in IONOLAB-TEC. The time intervals that are used to estimate the frequency and the duration of the disturbances are indicated with dashed blue lines and arrows.

In Tables 2 and 3, the frequencies and the durations corresponding to the time intervals in Fig. 7 are provided for Events 3 and 4, respectively. The frequencies and durations of the most significant disturbance are given as bold for the disturbances time intervals in Tables 2 and 3. As can be observed from Table 2, the frequencies during the LSTID (between 06.20 and 08.00 UT) are estimated as 0.16 MHz, 0.16 MHz and 0.83 MHz for colb, pktn and coso, respectively. The shortest period for LSTID is 20 min. The minimum duration is 90 min during LSTID. The most significant frequency component is lower than 1.0 MHz. In Table 2, between 01.00 and 08.00 UT, both colb and pktn stations observed the same frequency and duration of the disturbance. Between 14.00 and 20.00 UT, this time, pktn and coso had similar main frequency and duration values.

All of the frequency values during the reported MSTID time (between 03.30 and 06.10 UT) are higher than 1.0 MHz

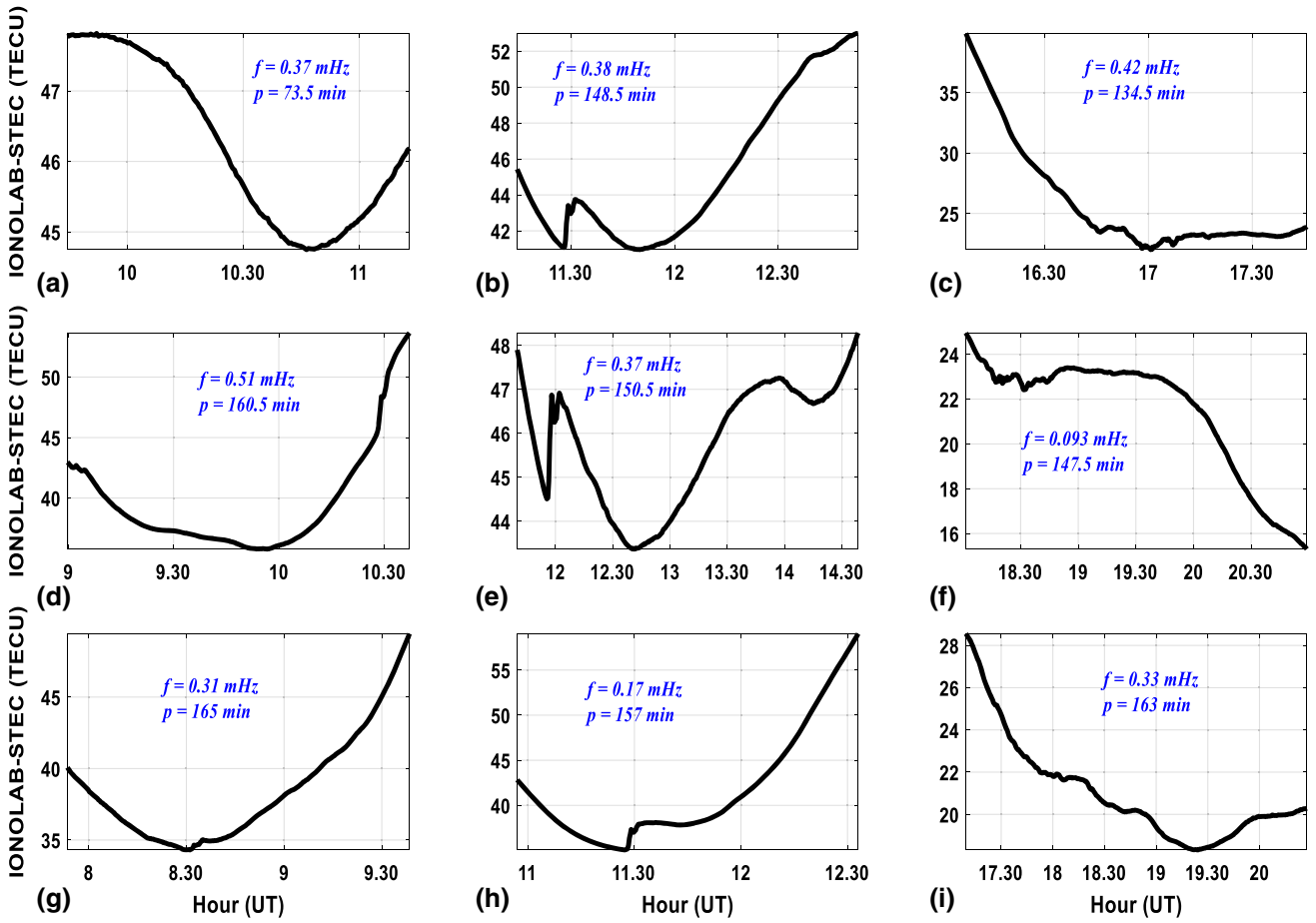

Fig. 5 Event 2, for station djig, IONOLAB-STEC during the time intervals of the peaks of SFs for: **a** PRN 26, **b** PRN 14, **c** PRN 22, **d** PRN 10, **e** PRN 27, **f** PRN 7, **g** PRN 18, **h** PRN 32 and **i** PRN 3. The most significant frequencies, *f*, and the durations, *p*, are given on the subplots

Table 2 Time intervals, frequencies and durations of the disturbances on October 29, 2003, Event 3, LSTID ('–' indicates no recorded GPS data at the station)

Station	Time intervals (UT)											
	01.00–06.20		06.20–08.00		08.00–14.00		14.00–20.00		20.00–23.59		00.00–23.59	
	f (mHz)	*p* (min)	*f* (mHz)	*p* (min)	*f* (mHz)	*p* (min)	*f* (mHz)	*p* (min)	*f* (mHz)	*p* (min)	*f* (mHz)	*p* (min)
colb	0.60	170	0.16	92.5	0.85	120	–	–	–	–	0.59	330
pktn	0.60	168	0.16	90	0.69	165	0.43	187.5	0.12	47.5	0.31	467.5
coso	1.07	65	0.83	92.5	0.092	230	0.46	127.5	0.40	17.5	0.83	92.5

as given in Table 3. According to Table 3, the longest period between 03.30 and 06.10 UT is 35 min. The durations during the reported MSTID in Table 3 are computed as 35 min, 27.5 min and 30 min for ccv3, pit1 and kyw1, respectively. When Tables 2 and 3 are considered, the scale of LSTID is observed to be significantly larger and the durations are longer as compared with those given for MSTID. The basis for the larger scale for LSTID than MSTID is the large-amplitude variations in TEC. During the LSTID, IONOLAB-TEC has reached up 150 TECU (Fig. 7c). The difference between the minimum and the maximum values of IONOLAB-TEC can reach up 142.2 TECU. IONOLAB-TEC has reached up 20 TECU during MSTID (Fig. 7f). The difference between the minimum and the maximum values of IONOLAB-TEC is 10.6 TECU. The dynamic level of TEC is very small during MSTID. Therefore, any wave-like or sudden disturbance, or an irregularity on TEC can be observed with higher frequencies and periods longer than 15 min. During LSTID, the dynamic level of TEC starts to increase with

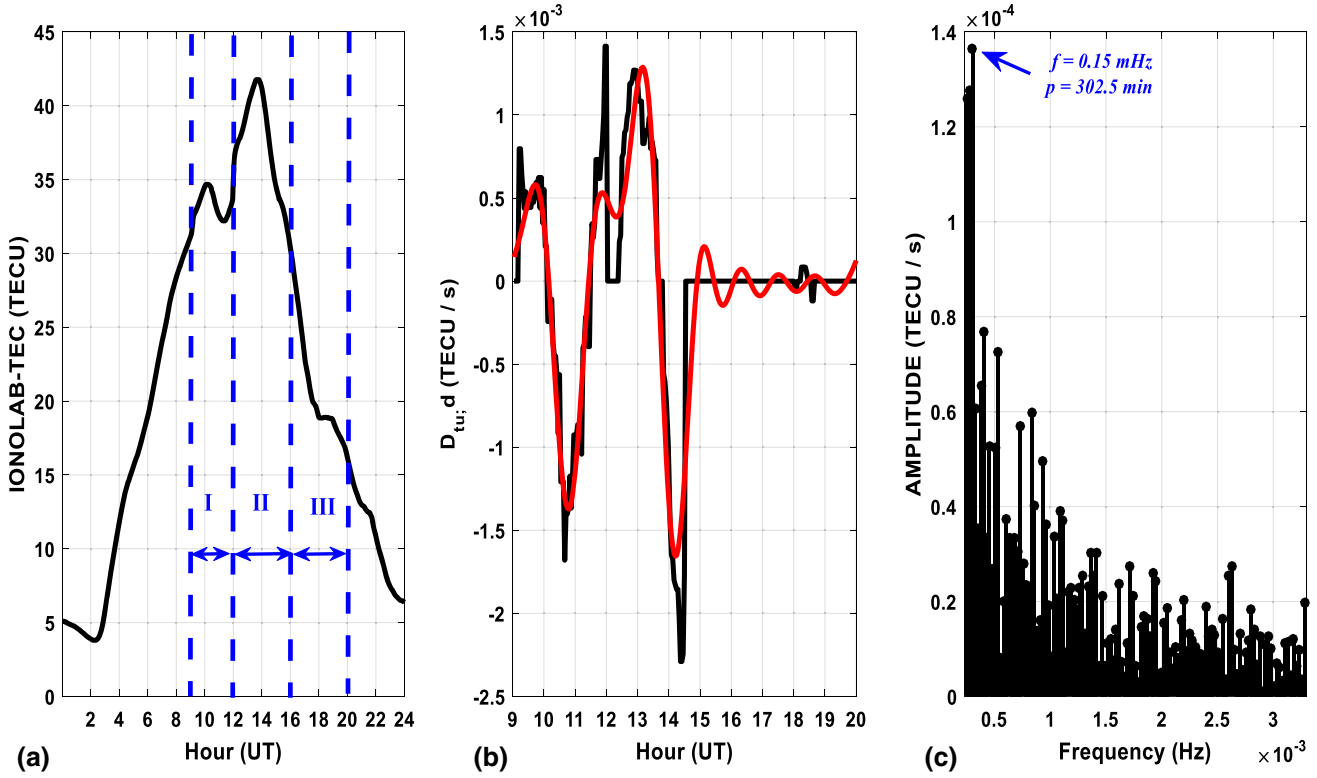

Fig. 6 Event 2, for station djig: **a** IONOLAB-TEC on September 06, 2017, **b** the smoothed derivatives of the difference, $\boldsymbol{D}_{t_{u;d}}$, (black) and summed sine functions, $\boldsymbol{S}_{u;d}$, (red) between 09.00 UT and 20.00 UT, **c** the spectrums, $\boldsymbol{F}_{u;d}$, between 09.00 UT and 20.00 UT. The dashed blue lines indicate the occurrence durations of the Solar Flares

Table 3 Time intervals, frequencies and durations of the disturbances on July 20, 2006, Event 45, MSTID

Station	Time intervals (UT)									
	01.00–03.30		03.30–06.10		06.10–13.00		13.00–23.59		00.00–23.59	
	f (mHz)	p (min)	f (mHz)	p (min)	f (mHz)	p (min)	f (mHz)	p (min)	f (mHz)	p (min)
ccv3	1.86	10	1.35	35	0.89	217.5	0.78	150	0.89	362.5
pit1	1.46	35	1.04	27.5	0.48	87.5	0.30	300	0.40	412.5
kyw1	1.86	12	1.56	30	0.89	227.5	0.91	207.5	0.78	450

lower frequencies and longer periods for any wave-like or sudden disturbances.

To investigate a possible wave-like disturbance during a seismic activity, Wenchuan (Sichuan) China earthquake is used as Event 5 given in Table 1. The earthquake occurred on May 12, 2008, at 06.28 UT. The location of the earthquake and the surrounding available GPS stations to the epicenter that are used for the Event 5 are given in Table 1. The effect of the earthquake has been easily observed on IONOLAB-STEC for the same PRNs for stations lhaz, xain and kunm after the earthquake. In Fig. 8a, c, e, IONOLAB-STEC values are given for PRN 14 for lhaz, xain and kunm, respectively. The earthquake time is demonstrated with a red arrow in the figures. On May 12, 2008, the frequencies and the durations for lhaz, xian and kunm and PRN 14 are estimated as follows:

- $f = 0.94$ mHz, $p = 197.5$ min (3.29 h)
- $f = 0.27$ mHz, $p = 177.5$ min (2.95 h)
- $f = 0.19$ mHz, $p = 170.5$ min (2.84 h)

May 12, 2008, is a geomagnetically quiet day. Maximum value of Kp index is 2 and Ap is 4. For Event 5, IONOLAB-TEC for May 12, 2008, is investigated into three time intervals. IONOLAB-TEC values are provided in Fig. 8b, d, f for lhaz, xian and kunm, respectively. The frequencies and the durations are computed for the pre-seismic, co-seismic and the post-seismic activity. These time intervals are indicated

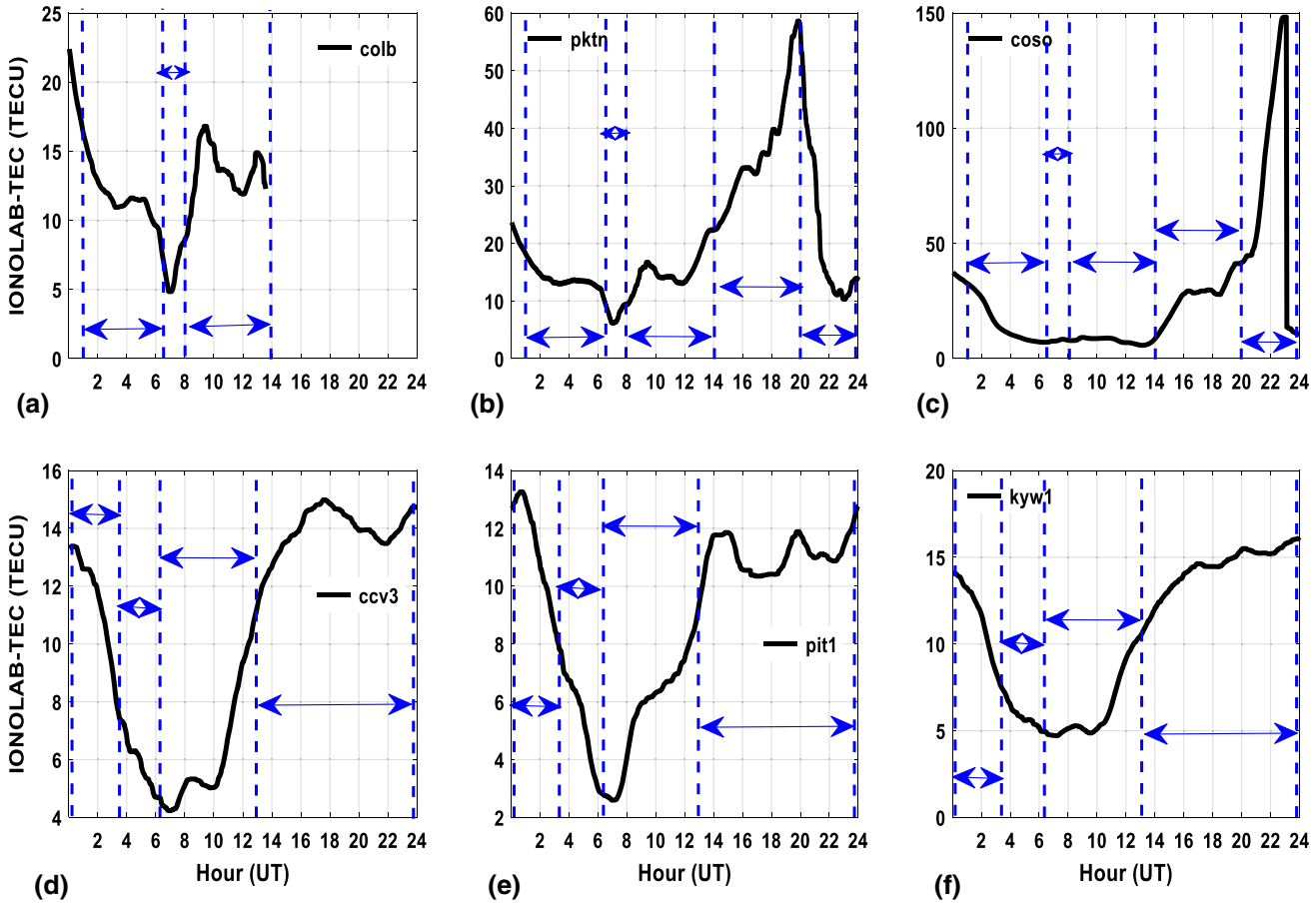

Fig. 7 Events 3 and 4; IONOLAB-TEC values for GPS stations: **a** colb, **b** pktn and **c** coso on October 29, 2003; and **d** ccv3, **e** pit1 and **f** kyw1 on July 20, 2006

Table 4 Time intervals, frequencies and durations of the disturbances during the earthquake on May 12, 2008, Event 5

Station	Time intervals (UT)							
	00.00–06.28		06.28–14.00		14.00–23.59		00.00–23.59	
	f (mHz)	p (min)	f (mHz)	p (min)	f (mHz)	p (min)	f (mHz)	p (min)
lhaz	1.26	25	0.075	315	0.64	195	0.22	490
xian	0.12	122.5	0.25	327.5	0.30	397.5	0.25	840
kunm	0.95	47.5	0.22	272.5	0.16	280	0.29	595

with dashed blue lines and double arrows in Fig. 8b, d, f. No frequency higher than 0.22 MHz is observed after the earthquake occurrence time between 06.28 and 14.00 UT. The minimum period in this time interval is 1 h 6 min. In Table 4, the estimated frequencies and durations of the disturbances are given for the periods 00.00–06.28 UT, 06.28–14.00 UT, 14.00–23.59 UT and for 24-h period.

In the second part of this section, IONOLAB-FFT is applied to five selected stations of TNPGN-Active, which lies in mid-latitude region between 36° and 42° N and 26° E and 45° E. The wave-like disturbances that are observed over IONOLAB-TEC are investigated for December (winter solstice), March (spring equinox), June (summer solstice) and September (autumn equinox) months in 2010 (low solar activity), 2011 and 2012 (moderate solar activity) in order to investigate the variability of fundamental frequencies of detrended IONOLAB-TEC. IONOLAB-TEC is computed with 2.5 min time resolution as discussed in Sect. 3.

In the low solar activity year, the dynamic level of TEC is very small. Although there is no geomagnetic storm in the region, any wave-like or sudden disturbance, or an irregularity on TEC can be observed with lower frequencies and periods longer than 1 h. Especially on near-solar minimum years, it is sensitive to oscillations or variabilities even up to 3 TECU. For the relatively geomagnetically quiet years, the TEC values are comparatively low, and thus, even

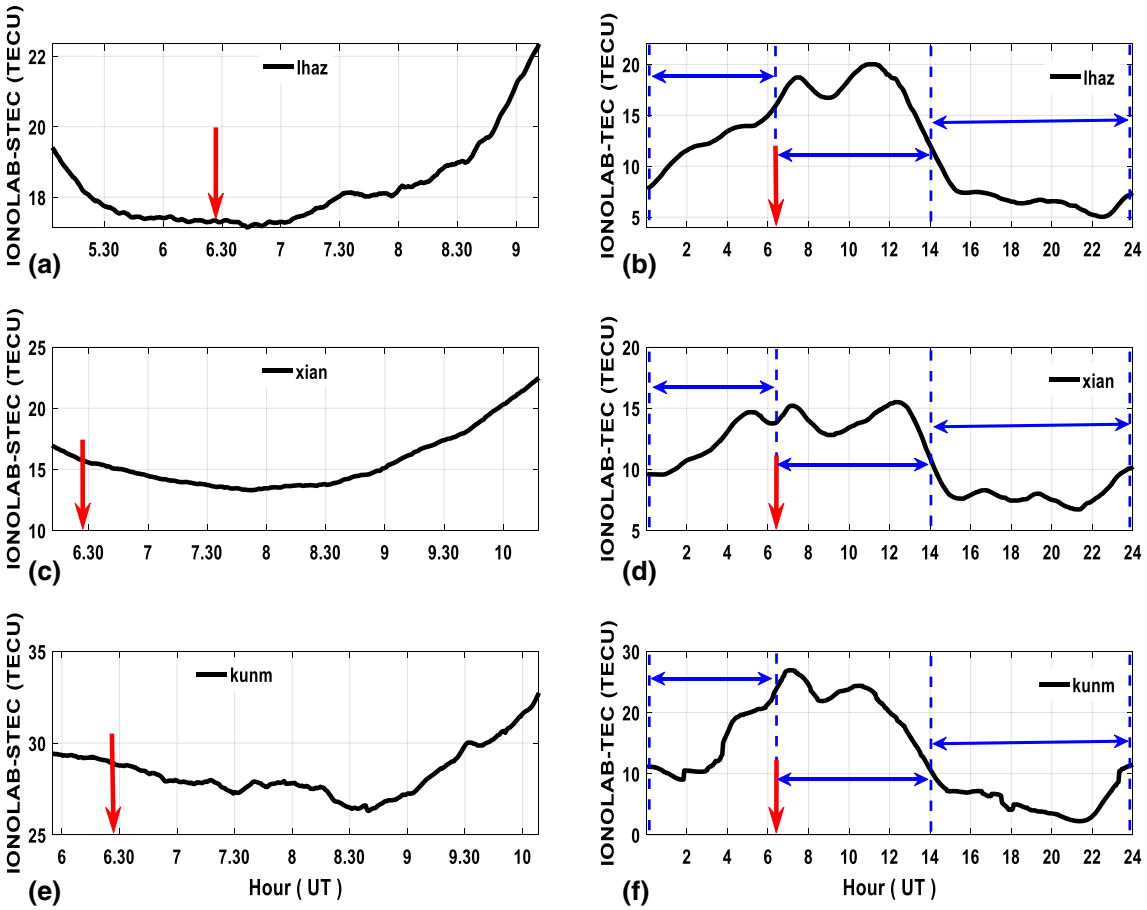

Fig. 8 Event 5, for lhaz: **a** IONOLAB-STEC for PRN 14, **b** IONOLAB-TEC; for xian: **c** IONOLAB-STEC for PRN 14, **d** IONOLAB-TEC; for kunm: **e** IONOLAB-STEC for PRN 14, **f** IONOLAB-TEC on May 12, 2008. The red arrows indicate the time of the earthquake in each figure

small-scale and lower-frequency disturbances with amplitudes up to 3 TECU can be detected as disturbances. As solar activity increases, TEC values also increase which enlarge the dynamic range during the diurnal cycle. In near-solar maximum years, lower frequencies and longer periods are indicators of severe disturbances, sudden enhancements or depletions due to possible geomagnetic storms or substorms in mid-latitude ionosphere. In Fig. 9a–c, IONOLAB-TEC values are provided for station band on September 25, 2010, 2011 and 2012, respectively. All 3 days are geomagnetically quiet days. Maximum values of Kp and Ap indices are 3 and 4, respectively. The frequency and the duration for 2010, low solar activity year, are 0.25 MHz and 445 min between 00.00 and 23.59 UT. The period of the disturbance is more than 1 h. With increasing solar activity after autumn equinox of 2011, the main frequency is greater than 0.50 MHz. The periods of the disturbances in moderate solar active years are less than 1 h. The durations of the disturbances between 00.00 and 23.59 UT are shorter than 200 min.

In order to observe the spatiotemporal distribution of wave-like disturbances or irregularities on TEC, IONOLAB-FFT method is applied to four special months and five selected stations in TNPGN-Active. For all stations and for all days during the chosen months of March, June, September and December, IONOLAB-FFT is applied to GPS-TEC for a whole day duration. All significant durations and frequencies are estimated according to the algorithm provided in Sect. 2. The estimated significant frequencies and durations are grouped into area-normalized bins, and experimental probability density functions (EPDFs) are obtained.

In Figs. 10a, 11a, 12a, the estimated most significant frequencies are presented as an EPDF for all 4 months and five stations and for 2010, 2011 and 2012, respectively. It is observed that the highest accumulation in Fig. 10a is around 0.08 MHz to 0.14 MHz corresponding to periods of 3.5 h to 2 h. In Fig. 11a, in 2011, the highest frequency probability occurs for 0.08 MHz to 0.1 MHz (3.5 h to 2.8 h). In 2012, in Fig. 12a, although the same range has the highest probability, the frequencies up to 0.14 MHz are also observed. In 2010 and 2012, the highest observed probable frequencies are 0.76 MHz corresponding to periods of 22 min (0.36 h). In 2011, the highest probability frequency bin range

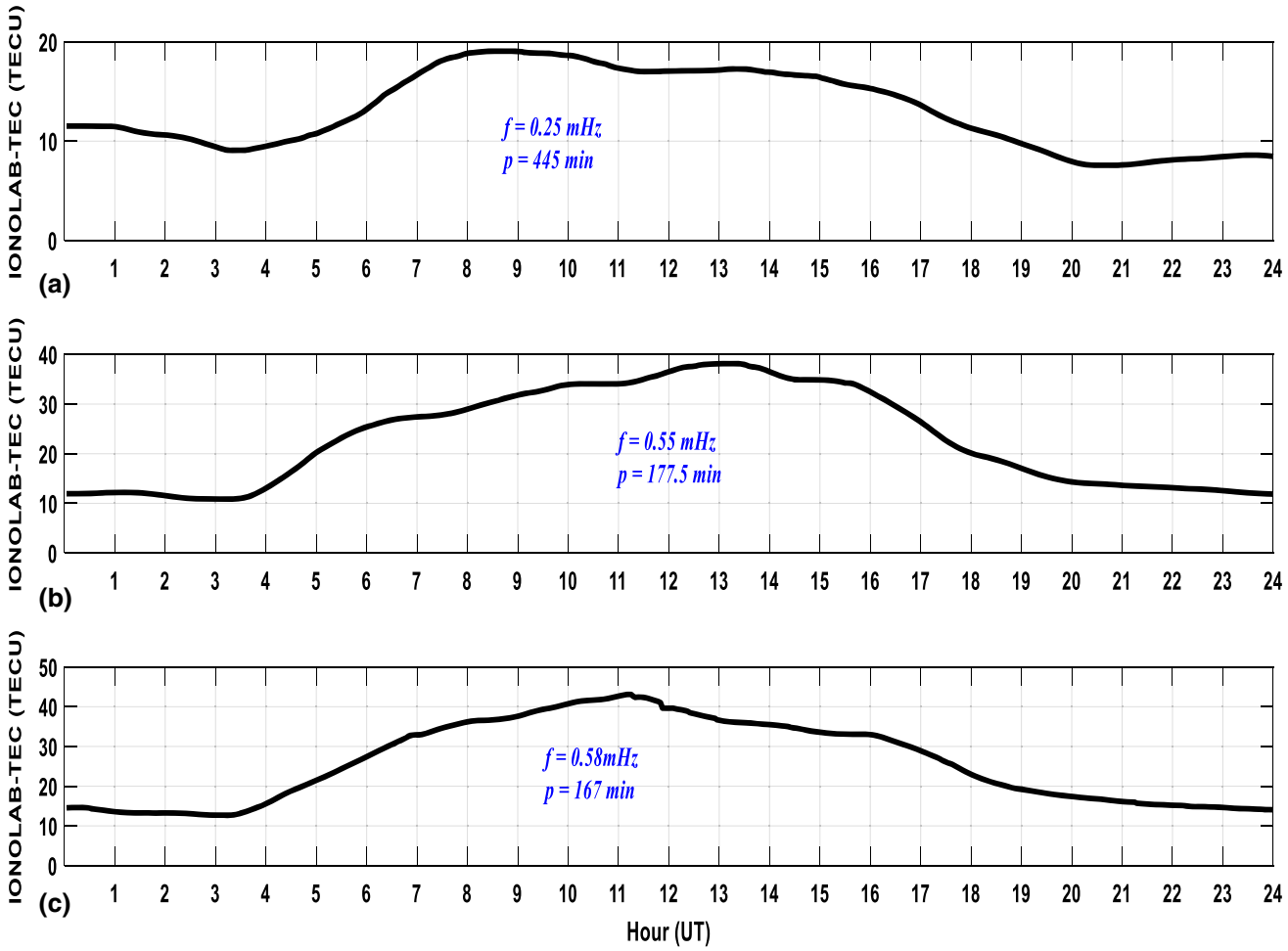

Fig. 9 IONOLAB-TEC values for band for: **a** September 25, 2010, **b** September 25, 2011, and **c** September 25, 2012

is 0.88 MHz (19 min or 0.32 h). 0.27 to 0.3 MHz corresponds to a period of 1 h. 0.28 MHz has a period of 59.5 min. In all years, it is observed that most frequencies are grouped less than 0.28 MHz (or periods larger than 1 h). The smallest frequencies are grouped around 0.02 MHz (period of about 14 h). The shortest periods are about 20 min. In March, June and September of 2010 (Fig. 10b–d, respectively), the most dominant frequency is 0.1 MHz, whereas in December 2010 (Fig. 1e), this range extends from 0.06 to 0.12 MHz. In 2011, in Fig. 11b–d, we observe similar peaks around 0.1 MHz, yet again, in December 2011, in Fig. 11e, the most common frequency is shifted to 0.075 MHz. In 2012, in all months given in Fig. 12b–e, the highest count is between 0.09 to 0.12 MHz (corresponding to periods of 3 h to 2.3 h). The highest frequencies are observed in December months of 2010, 2011 and 2012 along with September 2011.

In Figs. 13, 14 and 15, the EPDFs of all estimated durations are given for 2010, 2011 and 2012, respectively. As can be observed from the figures, a large number of the durations are between 425 and 550 min in 2010 (Fig. 13a), 300 and 550 min in 2011 (Fig. 14a), and 350 and 400 min in 2012 (Fig. 15a). The most significant durations are distinctly between 400 min (6.66 h) and 600 min (10 h) in March 2010 in Fig. 13b. In March 2011 (Fig. 14b), there is a more spread significant duration range from 300 min (5 h) to 450 min (7.5 h), whereas in March 2012 (Fig. 15b), the most significant duration range is very narrow, namely, from 350 min (5.83 h) to 400 min (6.66 h). In June 2010 (Fig. 13c), the significant frequency range is from 6.25 to 10 h. In June 2011 (Fig. 14c) and June 2012 (Fig. 15c), the same range is from 5 to 8.33 h. In September 2010 (Fig. 13d), the significant durations range from 7 to 9.1 h. For September 2011 (Fig. 14d), the same range is from 5 h to 6.66 h. A very wide range of significant durations (1.66 h to 6.66 h) is observed in Fig. 15d for September 2012. In December 2010 (Fig. 13e), the most significant durations are spread from 6.66 to 10.41 h. In December 2011 (Fig. 14e), the significant duration range is from 5 to 8.33 h, whereas in December 2012 in Fig. 15e,

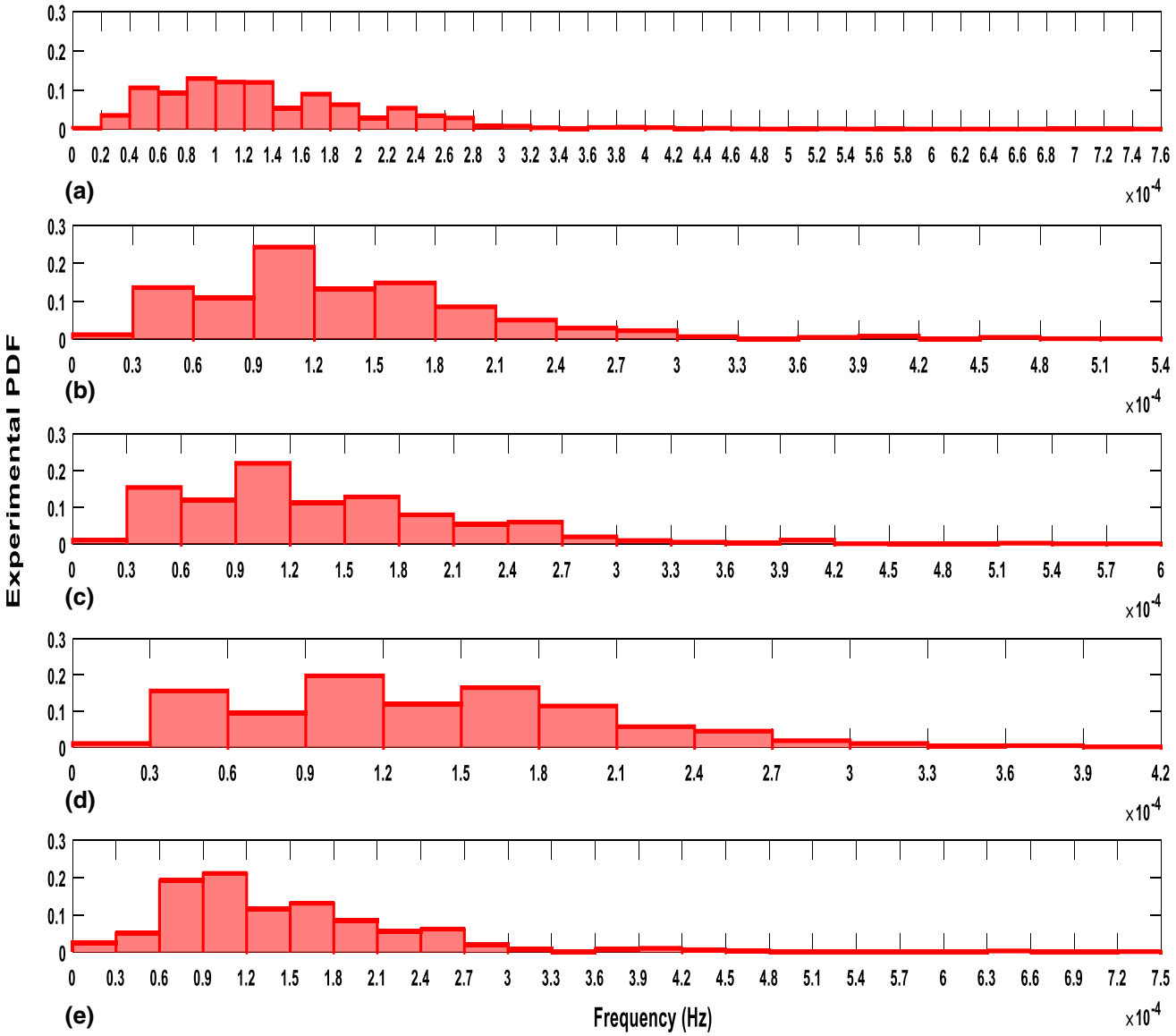

Fig. 10 The EPDFs of the estimated frequencies for: **a** March, June, September, December; **b** March; **c** June; **d** September; **e** December in 2010

this range is shortened to 7.5 h to 8.33 h. The longest duration is observed in March and December 2010, June and September 2011, and December 2012 around 800 min (13.33 h). The shortest duration (around 2 h) is observed in June, September, December of 2011 and June and September of 2012. In 2010, we have not observed any duration shorter than 200 min (3.33 h).

In Fig. 16, EPDFs of estimated frequencies with respect to five stations are given for the 4 months in 2010, 2011 and 2012. In the literature (Rishbeth et al. 2000; Azpilicueta et al. 2011; Gowtam and Ram 2017), if the global mean TEC values are larger for equinoxes than for solstices, it is called as semi-annual anomaly. During the semi-annual anomaly, an annual asymmetry that causes larger mean global TEC during the December than the June solstice is observed (far larger than the 7% that would be expected from the change on the Sun–Earth relative distance). It is observed that maximum counts of frequencies accumulate around 0.1 MHz in spring equinox (Fig. 16a) while it accumulates around 0.25 MHz in winter solstice (Fig. 16d) for low solar active year 2010. It corresponds to the periods 2 h 46 min in spring equinox and 1 h 7 min in winter solstice. With increasing solar activity, in Fig. 16l, the maximum counts of frequencies accumulate around 0.1 MHz in the winter solstice and the periods of the disturbances increase. When Fig. 16a, e, i is compared with Fig. 16d, h, l, it is observed that maximum frequency range is up to 0.55 MHz in spring equinoxes while it is up to 0.9 MHz in winter solstices. When the solstices are com-

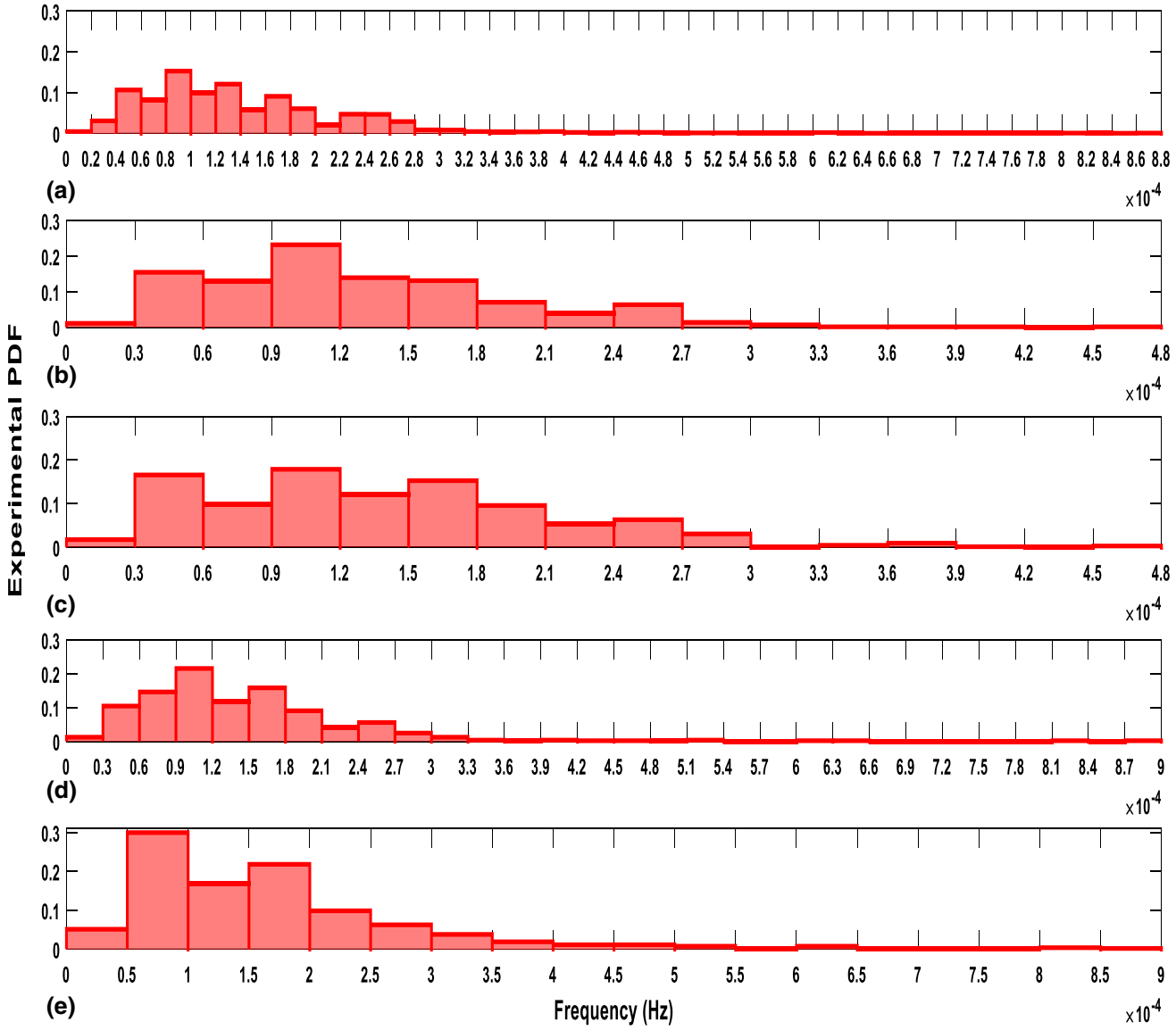

Fig. 11 The EPDFs of the estimated frequencies for: **a** March, June, September, December; **b** March; **c** June; **d** September, **e** December in 2011

pared with each other, it is observed that the frequencies in December months vary in a narrower range than those in June solstices. This range is between 0.1 and 0.25 MHz for December and 0.05 MHz and 0.3 MHz for June. December estimated frequency values are significantly lower than June. Thus, the periods of the disturbances are greater in December solstices.

Another interesting feature that can be observed from Fig. 16 is that there is an anisotropy in the North–South and East–West directions for the March equinox and the December solstice and in the North–South and West–East directions for the September equinox and the June solstice. The highest accumulation in Fig. 16 is around 0.1 MHz corresponding period of 2 h 46 min independent of latitude and longitude for all 3 years. As can be observed from Fig. 16, there is a prominent TEC gradient in the North–South direction. The counts of the frequency lower than 0.15 MHz for the GPS stations band and ardh in the northern part of Turkey are more than that for the GPS stations antl and btmn in the southern. It shows the fact that there exists a strong relation between the ionospheric disturbances and the latitude. Also, a prominent TEC gradient can be observed in the longitudinal direction. The stations band and antl in the west of Turkey have too much counts of the frequencies lower than 0.15 MHz.

In Fig. 17, EPDFs of the estimated durations with respect to the five stations are given for the 4 months in 2010, 2011 and 2012. As can be observed from Fig. 17, the estimated durations are predominantly accumulated around 300 min

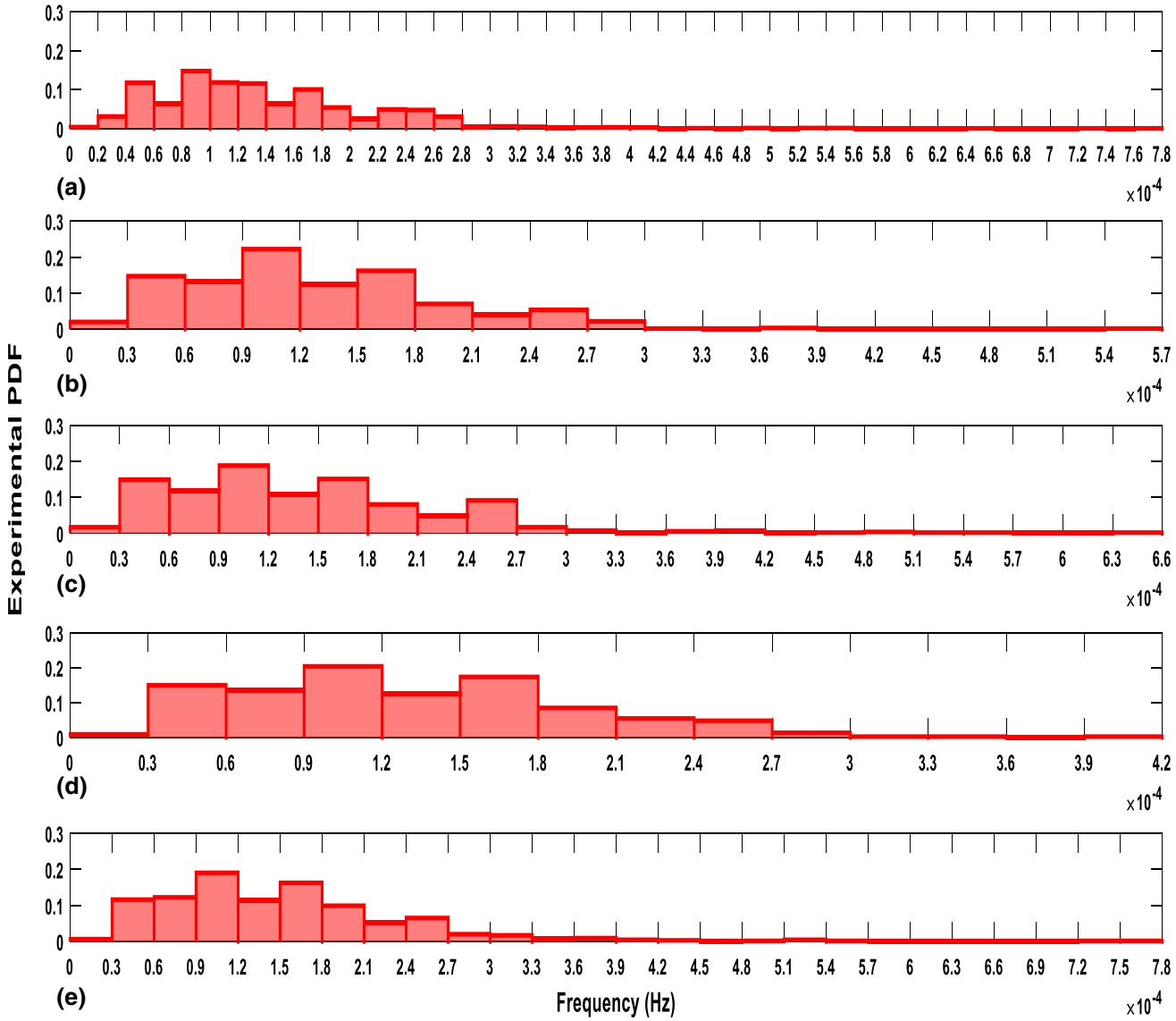

Fig. 12 The EPDFs of the estimated frequencies for: **a** March, June, September, December; **b** March; **c** June; **d** September; **e** December in 2012

and 400 min. In solar quiet year 2010, the durations of the disturbances last up to 900 min for all 4 months. In more active years 2010 and 2011, the durations are up to 800 min. For equinoxes (Fig. 17a, c, e, g, i, k), a large number of the durations are between 300 and 400 min while they are between 400 and 500 min for the solstices (Fig. 17b, d, f, h, j, l). With the increasing solar activity, disturbance durations decrease. During solar active year, the patterns are very different and they have an anisotropy. The spatial variability of the durations is larger for the north than for those in the south. This variability can be clearly observed from Fig. 17a, b. In both sub-figures, the large counts of the durations are observed for the stations band and anrk. In the west, the variability during the winter solstice is larger than those of the summer solstice. The results show that the disturbance duration increases with increasing latitude.

The results in this study indicate that mid-latitude ionosphere can exhibit a wide range of variability as a complicated function of SSN, geomagnetic and seismic activity, seasonal and meteorological changes. The geographical location of observation also seems to be factor. Both short-duration and small-amplitude disturbances, and long-duration and large-amplitude disturbances can be observed and classified using IONOLAB-FFT method. In the future studies, IONOLAB-FFT algorithm will be used as part of ionospheric monitoring systems in Turkey for detection of anomalies and disturbances that may cause problems in positioning and communication systems.

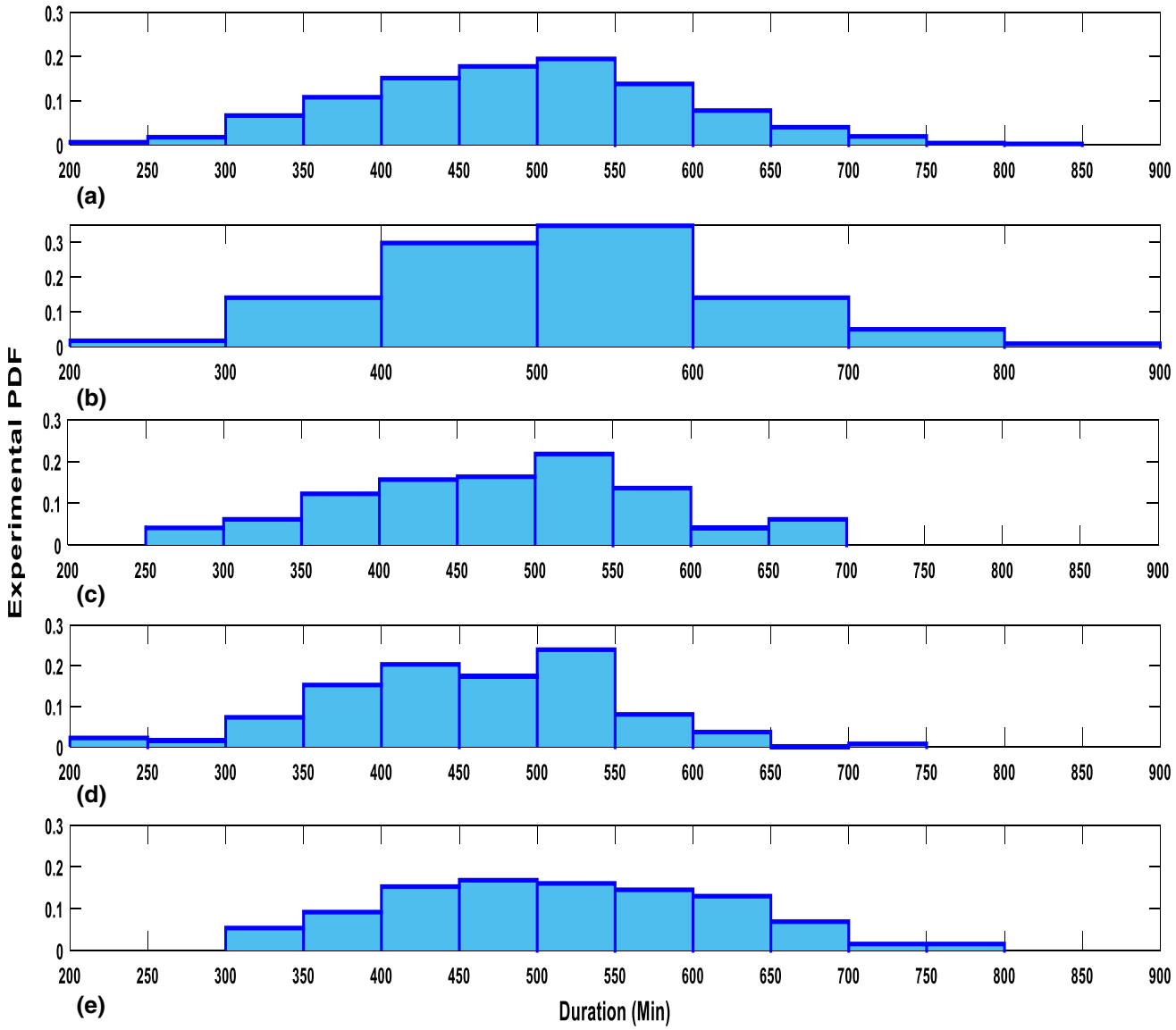

Fig. 13 The EPDFs of the estimated durations for: **a** March, June, September, December; **b** March; **c** June; **d** September; **e** December in 2010

5 Conclusion

In this study, in the first part, IONOLAB-FFT is modified to be applied to GPS-TEC data which is mentioned in the literature for various kinds of disturbances generated by a geomagnetic activity, a sudden ionospheric disturbance associated with a solar flare, a large-scale traveling ionospheric disturbance, a medium-scale traveling ionospheric disturbance and an earthquake. The frequencies and the durations of these different types of ionospheric disturbances are estimated using IONOLAB-FFT on the disturbance periods. During geomagnetically active period, the maximum value of the frequency is 0.48 MHz and it is lower than that for a quiet day. The maximum period of the disturbance in the geomagnetically disturbed day is approximately 3 h, and it corresponds to the duration described for LSTIDs in the literature. During a strong solar flare, the maximum frequency is observed in the less intensive flare and the value is lower than 0.5 MHz. The maximum period of the disturbance is 4 h, and it is observed during the most intensive flare on that day. When two events LSTID and MSTID are investigated, it is observed that maximum values of the frequencies are 0.83 MHz for LSTID and 1.56 MHz for MSTID. The periods of the disturbances are in accordance with those given for LSTID and MSTID in the literature. For the chosen earthquake, although the stations available for the study are distant to the epicenter, the effect of co- and post-seismic variability can still be observed. The maximum value of the frequency

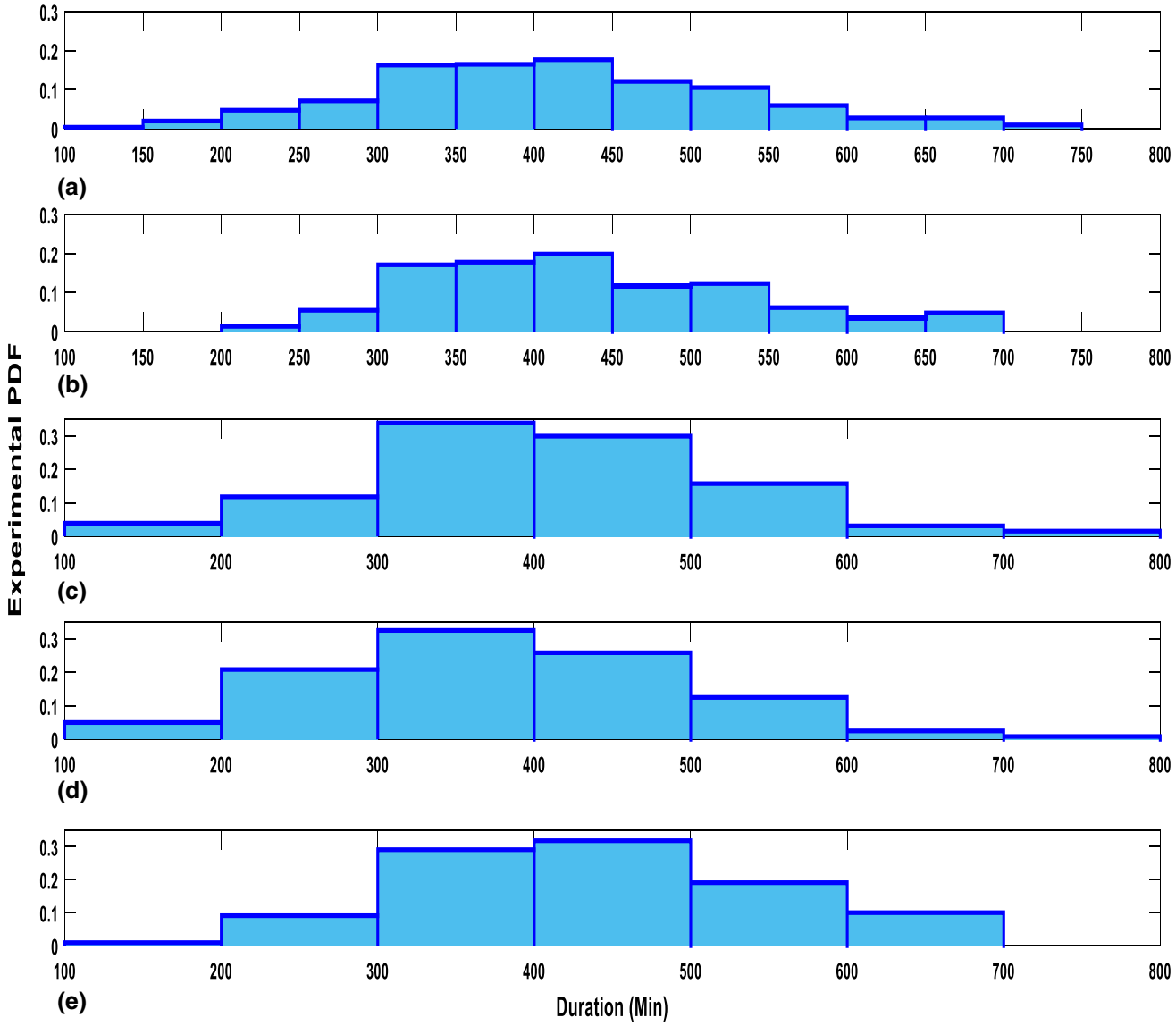

Fig. 14 The EPDFs of the estimated durations for: **a** March, June, September, December; **b** March; **c** June; **d** September; **e** December in 2011

for the stations with different distances to the epicenter is lower than 1.0 MHz during pre-, co- and post seismic activity on the earthquake day. The periods of the disturbances for three stations closely away from the earthquake center are 3 h 42 min, 1 h 7 min and 1 h 16 min after the earthquake time.

In the second part of the study, IONOLAB-FFT is applied to IONOLAB-TEC computed from TNPGN-Active located in mid-latitude region between 36° and 42° N and 26° E and 45° E in order to detect the any wave-like or sudden disturbance or irregularities during winter solstice, spring equinox, summer solstice and autumn equinox months in low solar active year 2010 and moderate solar active years 2011 and 2012. It is observed that a large number of the estimated frequencies are accumulated 0.08 MHz to 0.14 MHz in solar quiet year 2010 corresponding to periods of 3.5 h to 2 h. In 2011, the highest frequency count value is between 0.08 and 0.1 MHz corresponding to periods of 3.5 h to 2.8 h. In 2012, frequencies up to 0.14 MHz are also observed as dominant. In all years, it is observed that the most frequencies are grouped less than 0.28 MHz (or periods larger than 1 h). The smallest frequencies are grouped around 0.02 MHz (period of about 14 h). The shortest periods are about 20 min.

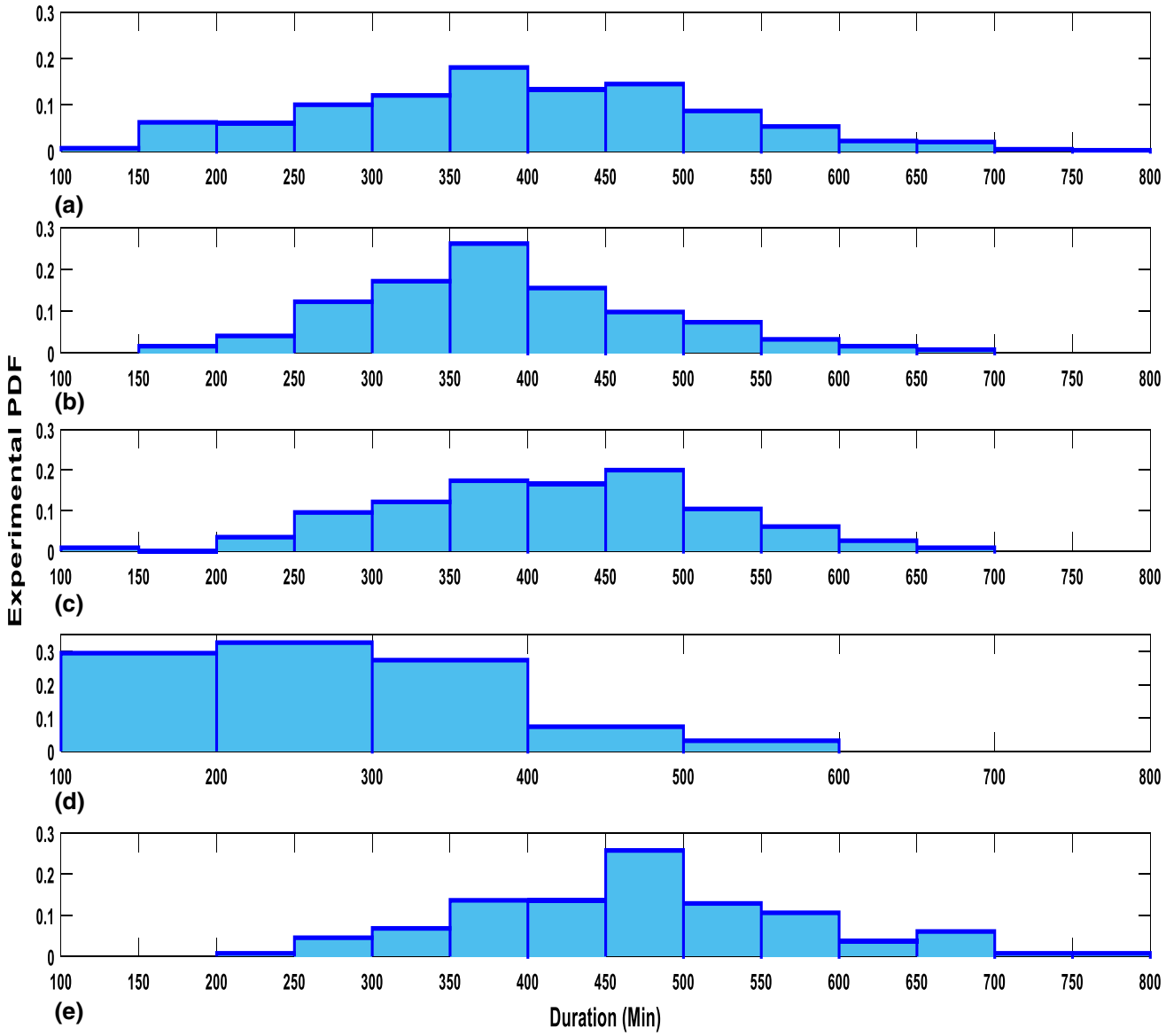

Fig. 15 The EPDFs of the estimated durations for: **a** March, June, September, December; **b** March; **c** June; **d** September; **e** December in 2012

A large number of the durations are between 425 and 550 min in 2010; between 300 and 550 min in 2011; and between 350 and 400 min in 2012. The longest duration is observed in March and December 2010, June and September 2011 and December 2012 around 800 min (13.33 h). The shortest duration (around 2 h) is observed in June, September, December of 2011 and June and September of 2012.

Based on these results, the IONOLAB-FFT algorithm can be used to estimate and characterize the frequency and the duration of wave-like oscillations. The results of this study will be used in modeling the statistical nature of mid-latitude ionosphere and possible classification of disturbances effective on positioning errors for ground-based augmentation systems.

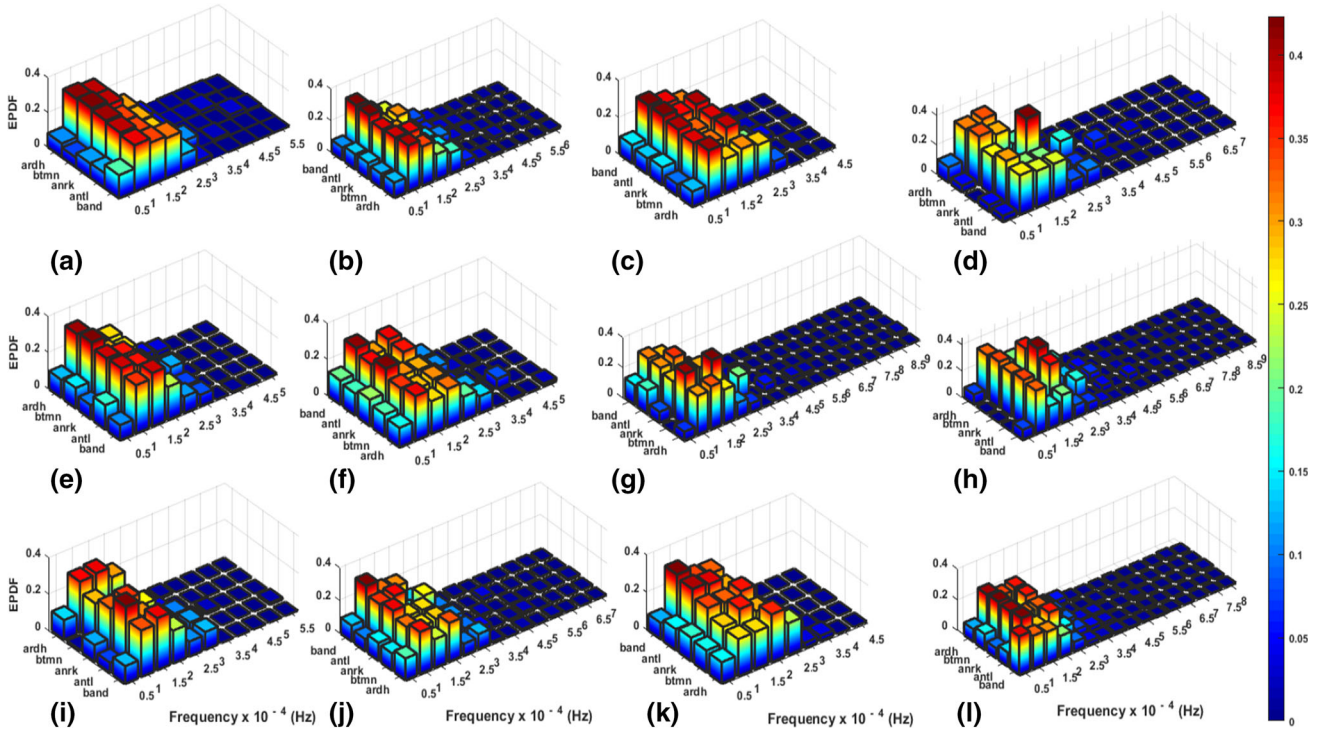

Fig. 16 EPDFs of estimated frequencies according to the stations and months: **a** March 2010, **b** June 2010, **c** September 2010, **d** December 2010; **e** March 2011, **f** June 2011, **g** September 2011, **h** December 2011; **i** March 2012, **j** June 2012, **k** September 2012, **l** December 2012

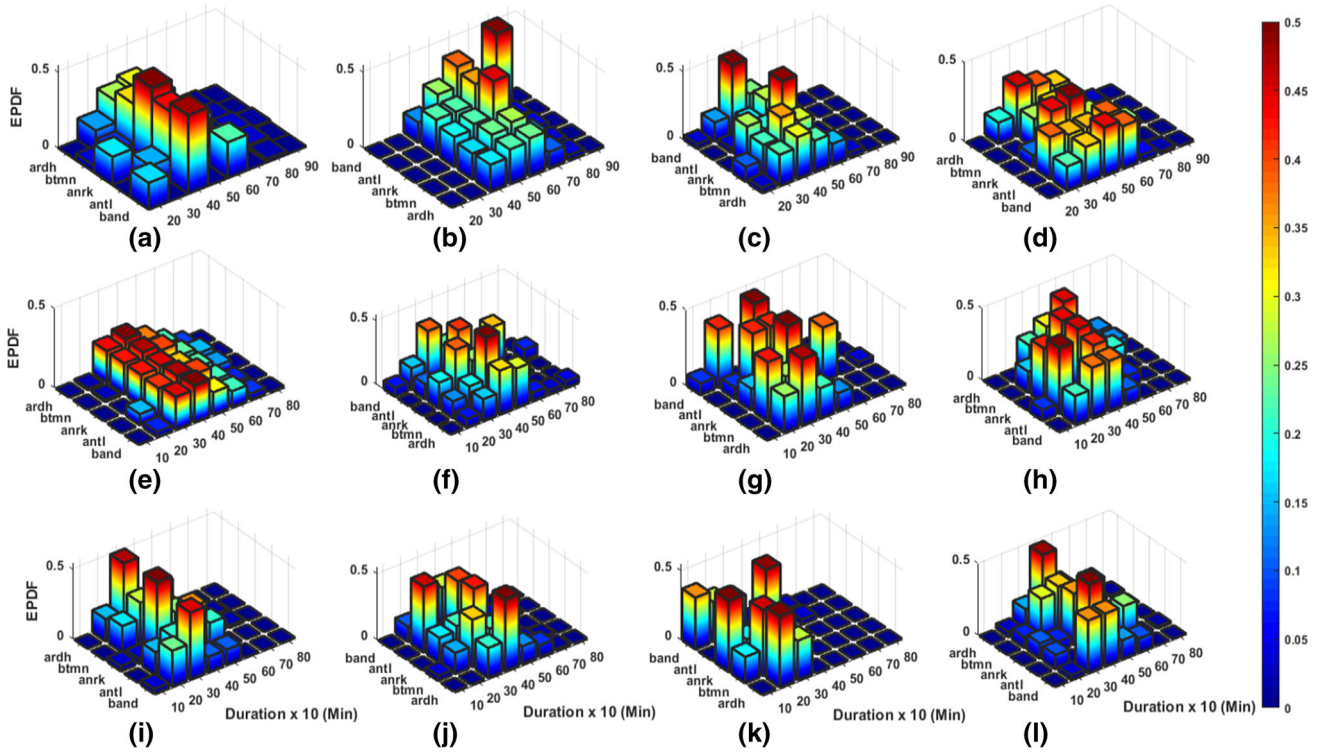

Fig. 17 EPDFs of durations according to the stations for: **a** March 2010, **b** June 2010, **c** September 2010, **d** December 2010; **e** March 2011, **f** June 2011, **g** September 2011, **h** December 2011; **i** March 2012, **j** June 2012, **k** September 2012, **l** December 2012

Acknowledgements This study is supported by TUBITAK 114E541, 115E915 and joint TUBITAK 114E092 and AS CR 14/001 projects. The GIM-TEC, Satellite DCB and ephemeris data that are used in computation of IONOLAB-TEC are obtained from IGS Analysis Center of Jet Propulsion Laboratory (JPL) at ftp://cddis.gsfc.nasa.gov/pub/gps/products/ionex. TNPGN-Active RINEX data set is made available to IONOLAB group for TUBITAK 109E055 project. This data set can be accessed by the permission from TUBITAK and General Command of Mapping of Turkish Army at https://www.hgk.msb.gov.tr/. The SSN data, Kp and Ap indices are obtained from National Oceanic and Atmospheric Administration (NOAA), U.S. Department of Commerce at ftp://ftp.swpc.noaa.gov/pub/indices/old_indices/. Earthquake information is obtained from https://earthquake.usgs.gov/earthquakes. AE and Dst indices are obtained from https://wdc.kugi.kyoto-u.ac.jp/. The TEC storm catalogs are obtained from Ionospheric Weather website of IZMIRAN at https://www.izmiran.ru/ionosphere/weather/storm/. The author is grateful to anonymous reviewers for their comments and contributions, which have been very helpful and constructive for the authors in improving the paper. Finally, the author wishes to thank Prof. Dr. Feza Arikan and IONOLAB group for their outstanding efforts on IONOLAB-BIAS and IONOLAB-TEC Algorithm.

Data availability All data sets used in this study are available from the references and relevant websites.

References

Afraimovich EL (2000) GPS global detection of the ionospheric response to solar flares. Radio Sci 35(N6):1417–1424

Arikan F, Yarici A (2017) Spectral investigation of traveling ionospheric disturbances: IONOLAB-FFT. Geodesy Geodyn 8(2017):297–304

Arikan F, Erol CB, Arikan O (2003) Regularized estimation of vertical total electron content from global positioning system data. J Geophys Res Space Phys 108(A12):1469–1480

Arikan F, Erol CB, Arikan O (2004) Regularized estimation of vertical total electron content from GPS data for a desired time period. Radio Sci 39(6):1–10

Arikan F, Arıkan O, Erol CB (2007) Regularized estimation of TEC from GPS data for certain mid-latitude stations and comparison with the IRI model. Adv Space Res 39:867–874

Arikan F, Nayir H, Sezen U, Arikan O (2008) Estimation of single station interfrequency receiver bias using GPS-TEC. Radio Sci 43(4):1–13

Arikan F, Sezen U, Toker C et al. (2016) Space weather studies of IONOLAB group. In: Proceedings of 2016 URSI Asia-Pacific radio science conference (URSI AP-RASC), Seoul, South Korea, August 2016, pp 1136–1139

Azpilicueta F, Brunini C, Radicella SM (2011) Semi-annual anomaly and annual asymmetry on TOPEX TEC during a full solar cycle. In: Proceedings of 2009 international-association-of-geodesy (IAG) scientific meeting, Buenos Aires, Argentine, July 2011, pp 769–774

Banks P, Kockarts G (1973) Aeronomy part B. Academic Press, San Diego

Basu S, Basu S, Valladares CE et al (2001) Ionospheric effects of major magnetic storms during the International Space Weather Period of September and October 1999: GPS observations, VHF/UHF scintillations, abd in situ density structures at middle and equatorial latitudes. J Geophys Res Space Phys 106(A12):389–413

Bergeot N, Chevalier JM, Bruyninx C et al (2014) Near real-time ionospheric monitoring over Europe at the Royal Observatory of Belgium using GNSS data. J Space Weather Space Clim 4(A31):1–10

Biqiang Z, Weixing W, Libo L, Tian M (2007) Morphology in the total electron content under geomagnetic disturbed conditions: results from global ionosphere maps. Ann Geophys 25(7):1555–1568

Brunini C, Camilion E, Azpilicueta F (2011) Simulation study of the influence of the ionospheric layer height in the thin layer ionospheric model. J Geodesy 85(9):637

Cherniak I, Zakharenkova I, Krankowski A (2014) Approaches for modeling ionosphere irregularities based on the TEC rate index. Earth Planets Space 66(165):1–5

Coster A, Williams J, Weatherwax A, Rideout W, Herne D (2013) Accuracy of GPS total electron content: GPS receiver bias temperature dependence. Radio Sci 48(2):190–196

Davies K, Baker DM (1965) Ionospheric effects observed around the time of the Alaskan earthquake of March 28, 1964. J Geophys Res 70(9):2251–2253

Davis MJ (1971) On polar substorms as the source of large-scale traveling ionospheric disturbances. J Geophys Res 76(19):4525–4533

Ding F, Wan W, Ning B, Wang M (2007) Large scale traveling ionospheric disturbances observed by GPS total electron content during the magnetic storm of 29–30 October 2003. J Geophys Res Space Phys 112(A6):1–15

Ding F, Wan W, Liu L, Afraimovich EL, Voeykov SV, Perevalova NP (2008) A statistical study of large-scale traveling ionospheric disturbances observed by GPS TEC during major magnetic storms over the years 2003–2005. J Geophys Res Space Phys 113(A3):1–8

Efendi E, Arikan F (2017) A fast algorithm for automatic detection of ionospheric disturbances: DROT. Adv Space Res 59(12):2923–2933

Erol CB, Arikan F (2005) Statistical characterization of the ionosphere using GPS signals. J Electromagn Waves Appl 19(3):373–387

Fedorenko YP, Fedorenko VN, Lysenko VN (2011) Parameters of the medium-scale traveling ionospheric disturbances model deduced from measurements. Geomagn Aeron 51(1):88–104

Fejer B, Farley D, Woodman R, Calderon C (1979) Dependence of equatorial F region vertical drifts on season and solar cycle. J Geophys Res 84(A10):5792–5796

Francis SH (1973) Acoustic-gravity modes and large-scale traveling ionospheric disturbances of a realistic, dissipative atmosphere. J Geophys Res 78(13):2278–2301

Gowtam SV, Ram ST (2017) Ionospheric annual anomaly—New insights to the physical mechanisms. J Geophys Res Space Phys 122(8):8816–8830

Hargreaves JK (1992) The solar-terrestrial environment. Cambridge University Press, Cambridge

Hernandez-Pajares M, Juan JM, Sanz J (2006) Medium-scale traveling ionospheric disturbances affecting GPS measurements: spatial and temporal analysis. J Geophys Res Space Phys 111(A7):1–13

Ho CM, Mannucci AJ, Sparks L et al (1998) Ionospheric total electron content perturbations monitored by the GPS global network during two northern hemisphere winter storms. J Geophys Res Space Phys 103(A11):26409–26420

Hocke K, Schlegel K (1996) A review of atmospheric gravity waves and travelling ionospheric disturbances: 1982–1995. Ann Geophys 14(9):917–940

Hsiao CC, Liu JY, Oyama KI et al (2010) Seismo-ionospheric precursor of the 2008 Mw7.9 Wenchuan earthquake observed by FORMOSAT-3/COSMIC. GPS Solut 14(1):83–89

Husin A, Abdullah M, Momani MA (2011) Observation of medium scale traveling ionospheric disturbances over Peninsular Malaysia based on IPP trajectories. Radio Sci 46(2):1–10

IONOLAB. www.ionolab.org

Jakowski N, Beniguel Y, De Franceschi G et al (2012) Monitoring, tracking and forecasting ionospheric perturbations using GNSS techniques. J Space Weather Space Clim 2(A22):1–14

Jianyong L, Guojie M, Xinzhao Y, Rui Z, Hongbo S, Yufei H (2015) Ionospheric total electron content disturbance associated with May 12, 2008, Wenchuan earthquake. Geodesy Geodyn 6(2):126–134

Jin S, Zhu W, Afraimovich E (2010) Co-seismic ionospheric and deformation signals on the 2008 magnitude 80 Wenchuan Earthquake from GPS observations. Int J Remote Sens 31(13):3535–3543

Karatay S, Arikan F, Arikan O (2010) Investigation of TEC variability due to seismic and geomagnetic disturbances in the ionosphere. Radio Sci 45(5):1–12

Karatay S, Cinar A, Arikan F (2017) Ionospheric responses during equinox and solstice periods over Turkey. Adv Space Res 60(9):1958–1967

Katamzi ZT, Smith ND, Mitchell CN, Spalla P, Materassi M (2012) Statistical analysis of travelling ionospheric disturbances using TEC observations from geostationary satellites. J Atmos Solar Terr Phys 74:64–80

Kil H, Paxton LJ, Pi X, Hairston MR, Zhang Y (2003) Case study of the 15 July 2000 magnetic storm effects on the ionosphere-driver of the positive ionospheric storm in the winter hemisphere. J Geophys Res 108(A11):1–22

Klobuchar JA (1987) Ionospheric time-delay algorithm for single-frequency GPS users. IEEE Trans Aerosp Electron Syst AES 23(3):325–331

Krankowski A, Shagimuratov II, Baran LW, Ephishov II (2005) Study of TEC fluctuations in Antarctic ionosphere during storm using GPS observations. Acta Geophys Polon 53(2):205–218

Krankowski A, Shagimuratov II, Baran LW, Ephishov II, Tepenitzyna NJ (2006) The occurrence of polar cap patches in TEC fluctuations detected using GPS measurements in southern hemisphere. Adv Space Res 38(11):2601–2609

Lastovicka J (2009) Lower ionosphere response to external forcing: a brief review. Adv Space Res 43(1):1–14

Ledvina BM, Makela JJ, Kintner PM (2002) First observations of intense GPS L1 amplitude scintillations at mid-latitude. Geophys Res Lett 29(14):1–4

Lin JW (2014) Ionospheric precursor of 2008 China Wenchuan earthquake using two-dimensional principal component analysis. HKIE Trans 21(3):192–194

Liu JY, Chuo YJ, Shan SJ et al (2004) Pre-earthquake ionospheric anomalies registered by continuous GPS TEC measurements. Ann Geophys 22(5):1585–1593

NASA's Goddard Space Flight Center. ftp://cddis.gsfc.nasa.gov/gps/products/ionex/

Nayir H, Arikan F, Arikan O, Erol CB (2007) Total electron content estimation with Reg-Est. J Geophys Res Space Phys 112(A11):1–11

Nicolls MJ, Kelley MC, Coster AJ, Gonzlez SA, Makela JJ (2004) Imaging the structure of a large-scale TID using ISR and TEC data. Geophys Res Lett 31(9):1–4

Ohki M, Zervakis ME, Venetsanopoulos AN (1995) 3-D Digital filters. Control Dyn Syst 69:49–88

Pi X, Mendillo M, Hughes WJ et al (2000) Dynamical effects of geomagnetic storms and substorms in the middle-latitude ionosphere: an observational campaign. J Geophys Res 105(A4):7403–7417

Prieto-Cerdeira R, Orús Pérez R, Breeuwer E, Lucas-Rodriguez R, Falcone M (2014) Performance of the Galileo single-frequency ionospheric correction during in-orbit validation. GPSworld 25:53–58

Pulinets SA, Contreas AL, Bisiacchi-Giraldi G, Ciraolo L (2005) Total electron content variations in the ionosphere before the Colima, Mexico, earthquake of 21 January 2003. Geofís Int 44(4):369–377

Pulinets SA, Kotsarenko AN, Ciraolo L, Pulinets IA (2007) Special case of ionospheric day-to-day variability associated with earthquake preparation. Adv Space Res 39(5):970–977

Rishbeth H, Garriott OK (1969) Introduction to ionospheric physics. Academic Press, New York

Rishbeth H, Mendillo M (2001) Patterns of F2-layer variability. J Atmos Solar Terr Phys 63(2001):1661–1680

Rishbeth H, Muller-Wodarg CF, Zou L et al (2000) Annual and semiannual variations in the ionospheric F2-layer: II Physical discussion. Ann Geo Phys 18:945–956

Roma-Dollase D, Hernández-Pajares M, Krankowski A et al (2018) Consistency of seven different GNSS global ionospheric mapping techniques during one solar cycle. J Geodesy 92:691–706

Russian Academy Sciences Izmiran. https://www.izmiran.ru/ionosphere/weather/storm/

Sagir S, Karatay S, Atici R, Yesil A, Ozcan O (2015) The relationship between the Quasi Biennial Oscillation and Sunspot Number. Adv Space Res 55(1):106–112

Sardon E, Rius A, Zarraoa N (1994) Ionospheric calibration of single frequency VLBI and GPS observations using dual GPS data. J Geodesy 68(4):230–235

Sayin I, Arikan F, Akdogan KE (2010) Optimum temporal update periods for regional ionosphere monitoring. Radio Sci 45(6):1–9

Sezen U, Arikan F, Arikan O, Ugurlu O, Sadeghimorad A (2013) Online, automatic near-real time estimation of GPS-TEC: IONOLAB-TEC. Space Weather 11(5):297–305

Shiokawa K, Ihara C, Otsuka Y, Ogawa T (2003) Statistical study of nighttime medium-scale traveling ionospheric disturbances using mid-latitude airglow images. J Geophys Res Space Phys 108(A1):1–7

Song Q, Ding F, Yu T et al (2015) GPS detection of the coseismic ionospheric disturbances following the 12 May 2008 M79 Wenchuan earthquake in China. Sci China Earth Sci 58(1):151–158

Space Research Center. ftp://ftp.cbk.waw.pl/idce/quiet_days/q_d_days.ctl

Space Weather Live. https://www.spaceweatherlive.com/en/archive/2017/09/06/xray

Space Weather Prediction Center. ftp://ftp.swpc.noaa.gov/pub/indices/old_indices/ftp://ftp.swpc.noaa.gov/stp/space-weather/solar-data/solar-indiceshttp://satdat.ngdc.noaa.gov/

Sripathi S, Balachandran N, Veenadhari B, Singh R, Emperumal K (2013) Response of the equatorial and low-latitude ionosphere to an intense X-class solar flare (X7/2B) as observed on 09 August 2011. J Geophys Res Space Phys 118:2648–2659

Stankov SM, Warnant R, Stegen K (2009) Trans-ionospheric GPS signal delay gradients observed over mid-latitude Europe during the geomagnetic storms of October–November 2003. Adv Space Res 43(9):1314–1324

Tsugawa T, Otsuka Y, Coster AJ, Saito A (2007) Medium-scale travelling ionospheric disturbances detected with dense and wide TEC maps over North America. Geophys Res Lett 34(22):1–5

Tsurutani B, Judge DL, Guarnieri FL et al (2005) The October 28, 2003 extreme EUV solar flare and resultant extreme ionospheric effects: comparison to other Halloween events and the Bastille Day event. Geophys Res Lett 32(L03S09):1–4

U.S. Geological Survey. https://earthquake.usgs.gov/earthquakes

Vlasov M, Kelley MC (2000) Kil H (2003) Analysis of ground-based and satellite observations of F-region behavior during the great magnetic storm of July 15. J Atmos Solar Terr Phys 65(11–13):1223–1234

Wang M, Ding F, Wan W, Ning B, Zhao B (2007) Monitoring global traveling ionospheric disturbances using the worldwide GPS network during the October 2003 storms. Earth Planets Space 59(5):407–419

World Data Center For Geomagnetism, Kyoto. https://wdc.kugi.kyoto-u.ac.jp/dstdir/

Yasyukevich Y, Astafyeva E, Padokhin A, Ivanova V, Syrovatskii S (2018) The 6 September 2017 X-class solar flares and their impacts on the ionosphere, GNSS, and HF radio wave propagation. Space Weather 16(8):1013–1027

Yuan Y, Ou J (2001a) Auto-covariance estimation of variable samples (ACEVS) and its application for monitoring random ionospheric disturbances using GPS. J Geodesy 75:438–447

Yuan Y, Ou J (2001b) An improvement to ionospheric delay correction for single-frequency GPS users—the APR-I scheme. J Geodesy 75:331–336

Yuan Y, Wang N, Li Z, Huo X (2019) The BeiDou global broadcast ionospheric delay correction model (BDGIM) and its preliminary performance evaluation results. NAVIGATION 66:55–69

Zhang DH, Xiao Z (2003) Study of the ionospheric total electron content response to the great flare on 15 April 2001 using the International GPS Service network for the whole sunlit hemisphere. J Geophys Res Space Phys 108(A8):1–11

Zhang X, Xie W, Ren X, Li X, Zhang K, Jiang W (2017) Influence of the GLONASS inter-frequency bias on differential code bias estimation and ionospheric modeling. GPS Solut 21(3):1355–1367

Zhang B, Teunissen PJG, Yuan Y, Zhang X, Li M (2018) A modified carrier-to-code leveling method for retrieving ionospheric observables and detecting short-term temporal variability of receiver differential code biases. J Geodesy 93:19–28